Koch-Müller, M., Jahn, S., Birkholz, N., Ritter, E., Schade, U. (2016): Phase transitions in the system CaCO3 at high P and T determined by in situ vibrational spectroscopy in diamond anvil cells and first-principles simulations. - *Physics and Chemistry of Minerals*, *43*, 8, pp. 545—561.

DOI: http://doi.org/10.1007/s00269-016-0815-8

Phase transitions in the system $CaCO_3$ at high P and T determined by in situ vibrational spectroscopy in diamond anvil cells and first-principles simulations

Monika Koch-Müller[1], Sandro Jahn[1,2], Natalie Birkholz[1,3], Eglof Ritter[4], Ulrich Schade[5]

[1]Deutsches GeoForschungsZentrum GFZ, Section 3.3, Telegrafenberg, 14473 Potsdam, Germany

[2] Institut für Geologie und Mineralogie, Universität zu Köln, Greinstr. 4-6, 50939 Cologne, Germany

[3] Institut für Angewandte Geowissenschaften, Technische Universität Berlin, Ackerstr. 76, 13355 Berlin, Germany

[4] Humboldt Universität zu Berlin, Experimentelle Biophysik, Invalidenstr. 42, 10115 Berlin, Germany

[5] Helmholtz-Zentrum Berlin für Materialien und Energie GmbH, Methoden der Materialentwicklung, 12489 Berlin, Germany

E-mail: mkoch@gfz-potsdam.de

Abstract

The stability of the high-pressure $CaCO_3$ calcite (cc)-related polymorphs was studied in experiments that were performed in conventional diamond anvil cells (DAC) at room temperature as a function of pressure up to 30 GPa as well as in internally heated diamond anvil cells (DAC-HT) at pressures and temperatures up to 20 GPa and 800 K. To probe structural changes, we used Raman and FTIR spectroscopy. For the latter, we applied conventional and synchrotron mid-infrared as well as synchrotron far-infrared radiation. Within the cc-III stability field (2.2-15 GPa at room temperature, e.g., Catalli and Williams in Phys Chem Miner 32(5-6):412-417, 2005) we observed in the Raman spectra consistently three different spectral patterns: Two patterns at pressures below and above 3.3 GPa were already described in Pippinger et al. (Phys Chem Miner 42(1):29-43, 2015) and assigned to the phase transition of cc-IIIb to cc-III at 3.3 GPa. In addition, we observed a clear change between 5 and 6 GPa that is independent of the starting material and the pressure path and time path of the experiments. This apparent change in the spectral pattern is only visible in the low-frequency range of the Raman spectra-not in the infrared spectra. Complementary electronic structure calculations confirm the existence of three distinct stability regions of cc-III-type phases at pressures up to about 15 GPa. By combining experimental and simulation data, we interpret the transition at 5-6 GPa as a re-appearance of the cc-IIIb phase. In all types of experiments, we confirmed the transition from cc-IIIb to cc-VI at about 15 GPa at room temperature. We found that temperature stabilizes cc-VI to lower pressure. The reaction cc-IIIb to cc-VI has a negative slope of -7.0×10^{-3} GPa K^{-1}. Finally, we discuss the possibility of the dense cc-VI phase being more stable than aragonite at certain pressure and temperature conditions relevant to the Earth's mantle.

Introduction

Carbonates are the most abundant carbon-bearing minerals on Earth. They can be transported into the upper and lower mantle via subduction processes. Evidence for the presence of carbonates in the mantle comes from carbonate inclusions in diamonds from the lower mantle (e.g., Brenker et al. 2007). Knowledge of the stability of solid carbonates adapting different structures with increasing pressure and temperature is therefore of great importance to understand the structure and dynamics of the Earth. Experimental studies and predictions by theoretical calculations suggest the formation of new carbonate structures (e.g., Isshiki et al. 2004) at high pressure and temperature, some of them with carbon in tetrahedral coordination (Oganov et al. 2008; Boulard et al. 2011, 2015). In this study, we focus on the system $CaCO_3$.

Bridgman (1939) and following studies (e.g., Jamieson 1957; Merrill and Bassett 1975; Suito et al. 2001) showed that $CaCO_3$ in the calcite structure (cc-I) transforms to metastable cc-II (monoclinic) and cc-III (different structure proposals) at ≈ 1.5 and ≈ 2.2 GPa, respectively. Cc-IV and cc-V are low-pressure high-temperature disordered modifications (Mirwald 1976) and will not be considered here. In a shock wave study, Tyburczy and Ahrens (1986) proposed another high-pressure form of $CaCO_3$ labeled cc-VI whose existence was confirmed by Catalli and Williams (2005) by in situ high-pressure IR spectroscopy (but labeled by them as post-$CaCO_3$-III). According to the latter authors, the transition of cc-III to cc-VI is sluggish: It starts at $p > 13.5$ GPa and is completed at 25 GPa. In an in situ single-crystal diffraction study, Merlini et al. (2012) confirmed the transformation of cc-III to cc-VI at pressures above 15 GPa. In this and in a more recent study, Merlini et al. (2012, 2014) solved the enigma of the structures of the high-pressure polymorphs cc-III and cc-VI.

According to recent textbooks in mineralogy, the stable high-pressure phase of $CaCO_3$ is aragonite (e.g., Wenk and Bulakh 2004, phase diagram on page 295) as in the pressure range up to about 15 GPa, and it has a higher density than cc-II and cc-III. However, Merlini et al. (2012) showed that this is not the case for cc-VI: At 20, 30 and 40 GPa they observed that cc-VI has a higher density than aragonite (their Fig. 3). According to Merlini et al. (2012), cc-III is triclinic and occurs in two closely related

structural modifications: cc-III with 50 atoms in the unit cell and cc-IIIb with 20 atoms. Both structures are characterized by the presence of planar carbonate groups, which, in contrast to cc-I and cc-II, are no longer coplanar to each other. Merlini et al. (2012) speculate that the incorporation of smaller cations than calcium may stabilize cc-III over aragonite even to lower pressures. Merlini et al. (2014) provide experimental evidence that cc-III and cc-IIIb are two polymorphs that are experimentally stable in the range of the cc-III stability field. Pippinger et al. (2015) carried out a Raman scattering, X-ray and synchrotron diffraction study on $CaCO_3$ up to 6.5 GPa and 550 K. They found cc-IIIb to be stable at relatively low temperature and pressure adjacent to the cc-II field. According to them, cc-IIIb transforms to cc-III at 3.28 ± 0.14 GPa at ambient temperature. In isothermal compression experiments, they determined the phase boundary between cc-IIIb and cc-III with a Clausius-Clapeyron slope of $-33.9 \pm 0.4 \times 10^{-3}$ GPa K^{-1}. Above 15 GPa and up to the maximum pressure investigated (40 GPa), Merlini et al. (2012) observed the high-pressure polymorph cc-VI in their in situ single-crystal X-ray diffraction study. According to them, cc-VI is triclinic with ten atoms in the unit cell. The CO_3 groups are coplanar, but not layered as in the lower-pressure polymorphs. The calcium site has an irregular coordination of seven shorter Ca-O distances (2.1 and 2.3 Å) and two longer ones (2.5-2.6 Å). Merlini et al. (2012) pointed out that their structure proposal for cc-VI was the same as that predicted and called phase II by Oganov et al. (2006). Thus far, there are no studies about the effect of temperature on the stability of cc-VI.

The vibrational properties of carbonates in the calcite (cc-I) structure at ambient conditions are well known and understood with respect to the molecular motions involved. In general, the internal modes of the CO_3 molecular vibrations (ν_1, ν_3 symmetric and asymmetric stretching, respectively; ν_2 and ν_4, out-of and in-plane bending, respectively) are distinguished from the external modes (ν_6-ν_{10}; ν_{13}; ν_{14}), which are defined as motions of the CO_3 groups against the cations (White 1974). The Raman spectra of cc-III are complex as the number of resolved modes significantly increases. According to the results of Liu and Mernagh (1990): Nine Raman modes are described below 300 cm^{-1}, namely at 96.8, 103.7, 128.9, 135.7, 164.7, 199.9, 209.1, 220.0 and 267.7 cm^{-1}; three bands are described in the region of the

ν_4 mode, namely at 695, 733 and 741 cm^{-1} and the ν_1 band with a shoulder at the low-energy side at about 1100 cm^{-1}. Liu and Mernagh (1990) describe two distinctive types of Raman spectra of calcite-III (type A and type B) and concluded that they result from different crystallographic orientations. Merlini et al. (2012, 2014) showed that the two most stable structures are cc-IIIb and cc-III. Finally, Pippinger et al. (2015) were able in a combined X-ray diffraction and spectroscopic study to distinguish Raman spectra of cc-IIIb from those of cc-III (both have space group $P\bar{1}$). The spectral differences are at low wavenumbers, where the external modes occur. The differences are characterized by different shifts $\Delta\nu/\Delta P$ of the doublet bands at 96.8 and 103.7 cm^{-1}, which are determined as -0.18 and +1.23 cm^{-1} GPa^{-1} below 3.2 GPa, respectively, and which turn to shifts of +2.29 and +4.04 cm^{-1} GPa^{-1} above 3.3 GPa. In addition, the band at 165 cm^{-1} is split into two components above 3.3 GPa. They confirmed these observations in several high-pressure and also high-pressure and high-temperature series. However, in one pressure series, Pippinger et al. (2015) observed no changes in the spectra at about 3.3 GPa, but significant differences at pressures above 3.8 GPa, namely a triplicated ν_1 mode accompanied by an increased number of bands around 700 cm^{-1} (ν_4) and by an increased number of weak external modes. They explain the spectral changes as being due to polysynthetic twinning under pressure with the crystal composed of crystal domains with different degrees of twinning and different orientations.

Table 1 shows a compilation of existing vibrational studies of carbonates at high pressure as well as the corresponding maximum P and T. With the exception of the studies by Minch et al. (2010a) and Pippinger et al. (2015), there is a clear lack of spectroscopic data taken at simultaneous high pressure and high temperature. The assignment of spectral features, especially of new high-pressure phases is not straightforward, but can be supported by electronic structure calculations in the framework of density-functional perturbation theory (DFPT). Theoretical Raman and IR spectra of carbonates at ambient pressure and zero temperature have been reported, e.g., by Valenzano et al. (2007), Carteret et al. (2013) and on www.wurm.info (Caracas and Bobocioiu, 2011).

To our knowledge, neither Raman nor far-infrared spectra of cc-VI have been published so far nor

does a pressure- and temperature-dependent study of the vibrations exist. In this study, we have a closer look at the pressure- and temperature-induced changes in the $CaCO_3$ structure and stability in the pressure range of 2-30 GPa with an experimental as well as atomistic modeling approach. Specifically, we will examine the effect of temperature on the phase transition of cc-III to cc-VI, e.g., the Clausius-Clapeyron slope of the cc-III to cc-VI transition, and investigate in detail the pressure-induced behavior of cc-III-related polymorphs at pressures up to 15 GPa.

Methods

Experimental methods

We investigated the full vibrational behavior of $CaCO_3$ by studying mid- to far-infrared as well as Raman spectra as a function of P at ambient T and simultaneously at high P and T. For the Raman measurements, we used the Horiba Jobin-Yvon LabRam HR800 VIS spectrometer at GFZ equipped with a blue (473 nm) DPSS-laser and a green (532 nm) Nd:YAG laser. For mid-infrared measurements, we used the Vertex 80v FTIR spectrometer combined with a Hyperion 2000 microscope at GFZ. For the synchrotron based mid-infrared (SR-MIR) measurements, we used the Nicolet 870 FTIR spectrometer combined with a Continuum microscope, and for synchrotron based far-infrared measurements (SR-FIR), we used the Bruker IFS66v spectrometer combined with the custom-made FIR microscope (Mrosko et al. 2011; Koch-Müller et al. 2012) at the IRIS beamline of the BESSY II storage ring of the Helmholtz-Zentrum Berlin (HZB), Germany. The samples were either thin films of synthetic pure $CaCO_3$ and natural calcite with 1 mol% $MgCO_3$ (infrared) or single crystals (Raman) of the same material 1-3 μm in size (synthetic) or up to 20 x 20 μm in size (natural). The larger single crystals were oriented with the cleavage face perpendicular to the laser beam; the smaller one's most probably had the same orientation as the spectral intensities were comparable.

The following experiments were carried out:

1. We performed two series of mid-infrared high-pressure experiments (A and B) at GFZ in the spectral range of 500-2000 cm^{-1} on thin films of chemically pure $CaCO_3$ in cc-I structure. We used a

piston-cylinder Mao-type diamond anvil cell (DAC) with type II diamonds (600-µm culets), 300-µm gasket hole and argon as pressure medium (Table 2: experiments M2-MIR-I; ZHS-MIR-II). To ensure quasi-hydrostatic conditions, we followed the instruction of Wittlinger et al. (1997) and annealed the cell at 8 GPa to 120 °C for 0.5 h (see Koch-Müller et al. 2011). For details of the film preparation and handling of the DAC, see Mrosko et al. (2011);

2. In situ SR-FIR spectra as a function of pressure were measured at the HZB. We used the above-mentioned THz/FIR microscope adapted to a Bruker IFS/66v FTIR spectrometer, which allows measurements under vacuum down to the THz region. We performed two high-pressure series in the far-infrared spectral range of 50-700 cm^{-1} on thin films of chemically pure $CaCO_3$ in cc-I structure (M2-FIR-I; M2-FIR-II). We used petroleum jelly as pressure medium. For details of the film preparation and handling of the DAC, see Koch-Müller et al. (2012);

3. Raman spectroscopy (GFZ) was applied in compression experiments at ambient temperature using the internally heated diamond anvil cells (DAC-HT) described below, but heating was only applied for relaxing the cell (e.g., the cell was annealed at different pressures to 70-120 °C for 30 min). In these two experiments (DAC-HT-13C and DAC-HT-15), NaCl was used as pressure medium and pressure was generated with the gas membrane technique. The cell was equipped with low-fluorescence type II diamonds 400 µm in diameter, and we used a 200-µm hole in the rhenium gasket. Spectra were collected on crystals of the synthetic calcite (DAC-HT-13C) and on the natural sample (DAC-HT-15) from 75 to 500 and 1000 to 1200 cm^{-1}. Three Raman experiments at ambient temperature used argon as pressure medium, ruby crystals as pressure sensors and the natural calcite as sample (M3-14; M3-15; M3-17). We used the above-mentioned Mao-type DAC with low-fluorescence type II diamonds 400 µm in diameter and a 200-µm hole in the rhenium gasket. Spectra were collected from 75 to 1200 cm^{-1};

4. We extended the DAC high-*P* studies to simultaneously high *T* by using internally heated diamond anvil cells (DAC-HT). The cells can be used up to 1000 K and 60 – 70 GPa with different pressure media (salts, noble gases) and are equipped with a gas membrane (nitrogen) for pressure increase. We

collected mid-infrared spectra at GFZ using conventional IR source and at HZB using SR-MIR both as function of temperature and pressure. However, for most of the in situ measurements at high pressure and high temperature, the Raman spectrometer at GFZ was used. For the mid-infrared spectra, the FTIR microscopes at GFZ and BESSY II, Berlin, were modified to allow in situ fluorescence measurements for pressure and temperature determination. Therefore, a green laser and an ocean optics USB spectrometer were installed in the optical path of the spectrometer. As P and T sensors, we placed ruby and $SrB_4O_7:Sm^{2+}$ into the gasket holes and measured their laser-induced fluorescence spectra at each pressure and/or temperature increase. The $SrB_4O_7:Sm^{2+}$ were synthesized by us following the recipe of Kulshreshtha et al. (2006). According to Datchi et al. (2007) and Raju et al. (2011) the $^7D_0$ – $^5F_0$ fluorescence line of the $SrB_4O_7:Sm^{2+}$ (at 685.4 nm at ambient condition) shifts with pressure, but is nearly independent on temperature. Jing et al. (2013) recalibrated the pressure shift at high temperature and high pressure. They come to the conclusion that there is an overall negligible coupling effect of temperature and pressure on the wavelength shift, but only below 770 K and 35 GPa. At higher temperatures, they suggest a new calibration relation for the $^7D_0$ – $^5F_0$ fluorescence line of the $SrB_4O_7:Sm^{2+}$. Cr^{3+} R1 fluorescence of ruby (at 694.2 nm at ambient conditions) is also pressure dependent, but strongly dependent on temperature – both dependences are well understood and calibrated (e.g., Mao and Bell, 1986; Datchi et al. 2007). We used the Sm^{2+} fluorescence line for determining the pressure. Then, we determined the temperature using the pressure corrections for the P-induced shift in the ruby fluorescence to correct the ruby peak position to the room pressure value and calculated the temperature. Figure 1 shows representative fluorescence spectra of both sensors at about 14 GPa and up to 510 K. The DAC-HT was also equipped with a k-type thermocouple located close to the lower diamond. We did several temperature calibration runs at different pressures with reproducible results. The temperature outside the gasket hole was always lower then inside, and the difference decreases with temperature reaching a ΔT of about 50 K at 800 K. Using the DAC-HT, we undertook several pressure series in combination with Raman and FTIR spectroscopy. In all experiments but two (DAC-HT-6 and DAC-HT-12), the natural calcite was used. In DAC-HT-6 and

DAC-HT-12, we used the chemically pure synthetic calcite. The DAC was equipped with low-fluorescence type II diamonds 500 μm in diameter and a 200 μm hole in the rhenium gasket. Sodium chloride was used as pressure medium, and ruby as pressure sensor (all DAC-HT experiments see Table 2). To reduce non-hydrostatic conditions, the cell was annealed at constant low pressures to about 100 °C and held there for about 30 min.

Table 2 summarizes all experiments and some experimental results.

Computational methods

The thermodynamic stability and vibrational spectra of different $CaCO_3$ polymorphs were derived from electronic structure calculations in the framework of density-functional theory (DFT). All calculations were performed using the ABINIT code (Gonze et al. 2009). The exchange-correlation functional was treated in the local density approximation (LDA). The Kohn-Sham orbitals were expanded in plane wave basis sets up to a cutoff energy of 1900 eV. This high cutoff was chosen to ensure convergence of the computed vibrational frequencies. Nuclei and core electrons were represented by Troullier-Martins-type pseudopotentials (Troullier and Martins 1991). The reciprocal space was sampled using suitable Monkhorst-Pack k-point grids (Monkhorst and Pack 1976) generated by ABINIT to ensure convergence of the total energy and its derivatives. In a first step, lattice parameters and atomic positions of primitive cells of the different $CaCO_3$ polymorphs cc-I (space group $R\bar{3}c, Z = 2$ in the rhombohedral cell), cc-III (space group $P\bar{1}, Z = 10$), cc-IIIb (space group $P\bar{1}, Z = 4$), cc-VI (space group $P\bar{1}, Z = 2$), aragonite (space group $Pmcn, Z = 4$) and post-aragonite (space group $Pmmn, Z = 2$) were optimized at different pressures in the athermal limit (T = 0 K). Input structures for all phases were taken from the literature (Merlini et al. 2012; Oganov et al. 2006). The pressure range of interest extended from room pressure (approximated by 0 GPa) to 30 GPa. Structures of cc-I, cc-III and cc-IIIb were not mechanically stable at the highest pressures. The same was true for cc-VI at pressures below 5 GPa. To investigate the relative phase stability at low pressures, the geometry optimization for some polymorphs was extended to negative pressures (up to -5 GPa), which corresponds to the crystals being under hydrostatic tensile stress. Geometry optimization was stopped

when the maximum force acting on an individual atom and the maximum deviation of a stress tensor component from the desired value were lower than 5 x 10^{-5} a.u.

Starting from the optimized structures, phonon frequencies at the Γ point of the Brillouin zone and the Born effective charge tensors were computed using linear response DFPT (Baroni et al. 2001) as implemented in the ABINIT code (Gonze et al. 2009). For the comparison of the computed vibrational spectra with experimental IR spectra, the low-frequency dielectric permittivity tensor was derived from the response functions using the method of Gonze and Lee (1997) with a damping factor of 2 cm^{-1}. The imaginary part of this function is a first approximation to the IR spectrum (see, for example, Jahn and Kowalski 2014). Further, Raman susceptibility tensors were computed using the DFPT method described in Veithen et al. (2005), which is implemented in ABINIT and essentially derives the third derivative of the energy with respect to electric field and atomic displacement perturbations. Powder-averaged Raman intensities were derived from the Raman tensors using the procedure described, e.g., in Caracas and Bobocioiu (2011).

Results

Vibrational characteristics of the $CaCO_3$ polymorphs

Figure 2 shows selected spectra of the $CaCO_3$ polymorphs, while spectra of the whole pressure series are shown in Figs. 3 and 4. In Fig. 2a, b Raman spectra of the $CaCO_3$ polymorphs are plotted in the spectral range of 75-500 cm^{-1} (a) and 1000-1200 cm^{-1} (b). Figure 2c, d shows mid- and far-infrared spectra, respectively. At pressures below 1.6 GPa, we observed the spectral pattern of cc-I (Fig. 2), and at 1.9 GPa, the transition of cc-I to cc-II (Fig. 2c) (White 1974). The focus of this study is, however, the phase behavior of cc-III and cc-VI. Based on an X-ray diffraction study, Pippinger et al. (2015) propose the transition of cc-IIIb to cc-III at around 3.3 GPa at ambient temperature. Thus, the spectra taken between 2.3 and 3.3 GPa are assigned to cc-IIIb, and those between 3.4 and 4.5 GPa are assigned to cc-III (Fig. 2). Spectra taken at pressures > 15 GPa (Fig. 2) are assigned to cc-VI (e.g., Catalli and Williams 2005; Merlini et al. 2012).

Compared to the Raman spectrum of cc-I with just two bands, the spectra of cc-III and cc-IIIb show at least nine different bands below 300 cm^{-1} (e.g., Pippinger et al. 2015). The spectra are characterized by a doublet around 100 cm^{-1}, strong modes around 160 and between 250 and 300 cm^{-1} (Fig. 2a), and a single band at about 1100 cm^{-1} plus shoulder at the low-energy side (Fig. 2b). The Raman spectrum of cc-VI (Fig. 2) is characterized by changes in the low frequency region: The low frequency mode of cc-III disappears, and a broad new band between 150 and 200 cm^{-1} evolves in addition to a broad triplet around 300 and a band around 420 cm^{-1}. In the high-frequency region (Fig. 2b) the ν_1 mode of cc-VI is represented by one single band centered at about 1150 cm^{-1}. In Fig. 2c, the mid-infrared spectra of cc-II and cc-III show the same modes as described for cc-I, but with considerable band splitting, e.g., of the ν_3 band at about 1400 cm^{-1}. The spectrum of cc-II is characterized by the appearance of the ν_1 symmetric stretching mode, which occurs as doublet at about 1050 cm^{-1}. The mid-infrared spectra of cc-III and cc-VI are well known and described, e.g., in Catalli and Williams (2005). Figure 2d shows a selection of the far-infrared spectra taken on pure calcite at the synchrotron source BESSY II as a function of pressure. The spectrum at 1.2 GPa shows the far infrared active lattice modes characteristic for cc-I, and the observed bands correspond to ν_6-ν_{10}, respectively, of White (1974). The spectra at 2.3 and 4.0 GPa are according to the findings of Pippinger et al. (2015) assigned to cc-IIIb and cc-III, respectively. The spectrum at 26.5 GPa is taken within the cc-VI stability field and is characterized by the appearance of an intense lattice mode at 218 cm^{-1} and disappearance of the low-frequency mode at around 100 cm^{-1}.

Evolution of the pressure-induced vibrational changes at ambient temperature

Before applying pressure and temperature to determine the stability fields of the different calcite structures, we determine the transformation pressures at ambient temperature. To probe structural changes, we used conventional and synchrotron mid-infrared, synchrotron far-infrared and Raman spectroscopy to choose which experimental setup visualizes the phase transformations best and to learn through the spectral changes more about the structural changes. The Raman spectra are shown in

Fig. 3 and infrared spectra in Fig. 4. Interpretation of vibrational spectra of carbonates is difficult as the onset of the changes appears to be kinetically delayed and spectra may show pattern of two phases (high P and low P) (e.g., Santillán et al. 2003; Catalli and Williams 2005). Also decompression spectra should be avoided for stability studies as the high-pressure phases persist over a broader pressure range also at low pressure. However, after decompression to ambient pressure, the cc-I structure was always observed again.

Figure 3a-c show the evolution of the high-pressure Raman spectra of $CaCO_3$ taken in three different pressure series in small pressure intervals at ambient temperature and in the low-frequency region. Figure 3d-f show the same pressure series, but at high frequencies (1000-1200 cm^{-1}). The spectra in Fig. 3a, d (DAC-HT-15) and 3c, f (DAC-HT-16) were taken on natural calcite, and those in Fig. 3b, e (DAC-HT-13C) on 1-3 μm small synthetic pure $CaCO_3$ as starting material. Within the cc-III stability field (2.2-15 GPa at room temperature, e.g., Catalli and Williams (2005)), we observed in the Raman spectra three different spectral patterns. Two patterns are already described and shown in Fig. 2a for cc-IIIb and cc-III. At pressures between 5 and 6 GPa and ambient temperature, we observed another more abrupt change in the Raman pattern. In the spectra at 5.7 GPa (Fig. 3a), 8.3 GPa (Fig. 3b) and 7.9 GPa (Fig. 3c), the doubled bands around 100 cm^{-1} are disappeared, and we observe an intense band between 120 and 130 cm^{-1}, and a very weak one at about 105 cm^{-1}. The band at about 120 cm^{-1} (5.7 GPa) first shifts slightly with increasing pressure to higher wavenumbers and from 9.5 GPa to lower wavenumber (Fig. 3a). The new low-frequency mode at around 105 cm^{-1} does not shift with increasing pressure, but decreases in intensity until it disappears when cc-VI is formed. In contrast to Fig. 3a and b, this band disappears in the spectra of experiment DAC-HT-16 (Fig. 3c) already at 11.2 GPa. In addition, from 12 GPa, the new band at about 125 cm^{-1} starts to decrease in intensity with increasing pressure until it also disappears at about 15.3 GPa, and in parallel, the characteristic bands for cc-VI at about 150 and 190 cm^{-1} start to increase in intensity from about 13.6 GPa to higher pressures (Fig. 3a). The high-frequency mode ν_1 (Fig. 3d-f) occurs at pressures below 5.6 GPa as singlet with a shoulder on the low-energy side as described by, e.g., Pippinger et al. (2015). From 5.6 GPa, a singlet evolves

with increasing pressure, which shifts to higher wavenumber (Fig. 3 d-f). No spectral changes during the transformation into cc-VI can be observed in this spectral range. In Fig. 3d, the high-frequency mode again turns to become a doublet at 13.6 and 14.5 GPa, and finally at pressure >21 GPa, it becomes a singlet again. All Raman spectroscopic pressure series gave more or less the same picture of three different spectral patterns in the range of 2.2-15 GPa (Fig. 2, 3). Figure 4a shows the mid-infrared spectra from 500 to 2000 cm^{-1} as a function of pressure (M2-MIR-I). According to Pippinger et al. (2015), the spectrum taken at 3.4 GPa is assigned to cc-III and is characterized by multiple mode splitting compared to the low-pressure polymorphs. In the spectra between11.3 and 15.1 GPa (Fig. 4a, a-1, a-2) four bands and strong change in the mode appearance can be observed for ν_1 (around 1100 cm^{-1}) and ν_2 (between 700 and 800 cm^{-1}). The second MIR pressure series showed comparable results. We distinguish four different spectral patterns in the FIR spectra (Fig. 2d and Fig. 4b): the far-infrared spectrum at 1.2 GPa (cc-I), the spectrum at 2.3 GPa (according to Pippinger et al. 2015 assigned to cc-IIIb), the spectra between 4.0 and 15.5 GPa (according to Pippinger et al. 2015 assigned to cc-III) and the spectra at pressures >19.8 GPa, which are according to Catalli and Williams (2005) assigned to cc-VI.

In two of the Raman-experiments (M3-14 and M3-M15), we obtained spectra after pressure increase from 2.1 to 9.5 GPa with an increased number of bands around 700 cm^{-1}, with an increased number of weak external modes and a triplicated ν_1 mode just the same as Pippinger et al. (2015) described for one of their runs (see their Fig. 4a, b). As mentioned before, they explain the spectral changes as polysynthetic twinning under pressure. After pressure release, the spectrum of the recovered sample showed the pattern of perfect crystalline cc-I. All other spectral changes with increasing pressure as observed in this study do not show a spectral pattern that could be assigned to pressure-induced twinning.

In situ high-pressure/high-temperature infrared and Raman spectroscopy using internally heated diamond anvil cells in the system $CaCO_3$

Considering the experimental data presented above, it seems that with Raman spectroscopy, the phase transitions can be traced best. As determined at ambient temperature (see above), the Raman cc-VI spectra are characterized by the disappearance of the band between 120 and 130 cm^{-1} and the appearance or intensification of the bands around 150 cm^{-1} and 200 cm^{-1}. Therefore, we preferably applied this method to determine the slope of the cc-III to cc-VI phase transition using the DAC-HT. However, some mid-IR spectra at high P and T were also collected at GFZ and at BESSY II using SR-MIR. According to Catalli and Williams (2005), the formation of cc-VI is indicated in infrared spectra by appearance of new bands of the v_4 mode. Starting with the cc-III structure at a certain pressure and ambient temperature either the temperature was increased until cc-VI was formed or isothermal compression was applied. Some experiments started also with the cc-VI structure and temperature was increased up to 658 K. All experiments are summarized in Table 2.

Figure 5a shows Raman spectra of the experiment DAC-HT-16 at high pressure and simultaneously high temperature. After pressure increase to 11.7 GPa, we started heating until 475 K without changing the pattern. Figure 5b shows mid-infrared spectra of run DAC-HT-12. The spectrum at 18.8 GPa (Fig. 5b and label 4 in Fig. 5c) is taken in the cc-VI stability field, and the spectrum has components of cc-III and cc-VI modes. The growing of cc-VI is indicated by the appearance of two new bands for the v_4 mode (Catalli and Williams 2005). One of them is indicated by (!) in Fig. 5c. Heating the sample under pressure until 441 K did promote the transformation to cc-VI (Fig. 5c). The next experiments were performed at pressure of about 14 GPa in combination with Raman spectroscopy, and the phase transition from cc-III to cc-VI could be observed in three different heating cycles (Fig. 6a, c). In Fig. 6c, the spectrum at 14.7 GPa and 306 K was taken immediately after temperature switch off and shows that cc-VI transformed back to cc-IIIb. Figure 1S (supplement material) illustrates again the transition of cc-IIIb to cc-VI by Raman spectroscopy at about 13.7 GPa and 543 K (Fig. 1Sa and 1Sb) and at 15 GPa and 522 K (Fig. 1Sc). In Fig. 1Sa, the Raman-active v_1 mode is shown, which seems to be not affected by the phase transition.

Electronic structure calculations

DFT simulations were performed to support the interpretation of the experimental data. Geometry optimization was first performed using pseudopotentials consistent with the Perdew-Zunger-Ceperley-Alder parameterization of LDA (Perdew and Zunger (1981); ABINIT option ixc = 2). The cell parameters of the relaxed structures at T = 0 K and a range of pressures for different $CaCO_3$ polymorphs are listed in Table 3. The respective enthalpies and cell volumes are shown in Fig. 7. At each pressure, the lowest enthalpy curve corresponds to the thermodynamically stable phase as predicted by the DFT model (Fig. 7a). Compared to the real $CaCO_3$ system, the stability field of cc-I is somewhat shifted to negative pressure (which corresponds to a system under tensile stress). Between -1.2 GPa and 30 GPa, aragonite is the most stable phase, followed by post-aragonite at higher pressures. The cc-III phases are more stable than cc-I above -0.9 GPa. The enthalpy curve of cc-IIIb changes slope between 0.5 GPa and 4 GPa, which leads to two (meta-)stability regions of cc-IIIb among the cc phases, i.e., between -0.9 and 0.0 GPa and between 5 and 14 GPa. This change in slope is reproducible on the compression and decompression paths. Cc-III has the lowest enthalpy of the cc phases between 0 and 5 GPa, whereas cc-VI is the most stable cc polymorph above 14 GPa. The molar volume decreases in the sequence cc-I > cc-IIIb (<2 GPa) > cc-III > cc-IIIb (>2 GPa) > aragonite > cc-VI > post-aragonite (Fig. 7b). The molar volumes of cc-IIIb and cc-III cross at about 2 GPa with cc-IIIb being less dense than cc-III below 2 GPa and denser above 2 GPa. Cc-VI has a higher density than aragonite, which is consistent with experimental observations (Merlini et al. 2012).

The calculation of Raman spectra with ABINIT requires the use of another formulation of LDA, e.g., Perdew and Wang (1992), ABINIT option ixc = 7. Therefore, we decided to re-optimize all of the structures for which vibrational spectra were derived subsequently. As shown in Table 3, both LDA flavors yield very similar results. The cell parameters and atomic positions of selected DFT-optimized structures used for the calculation of vibrational spectra are provided in the electronic supplement. Selected theoretical and experimental Raman spectra of cc-IIIb and cc-VI are shown and compared in Fig. 8. Due to somewhat different pressures and to the approximations inherent to the DFT

calculations, the frequencies of the theoretical spectra are slightly shifted with respect to the experimental data. We therefore focus our comparison on the relative positions of the bands with the highest Raman intensities. As in the experiments, the Raman spectra of cc-IIIb at pressures below and above the cc-III stability field (Fig. 8a, b) are rather similar with high intensity bands around 1100, 100 cm^{-1}, a number of medium-intensity modes between 150 and 400 cm^{-1}, and between 700 and 850 cm^{-1}. The main spectral features of the theoretical spectra can be assigned to bands of the experimental spectra. As the wavenumber range between 700 and 850 cm^{-1} was not covered in the present experiments, the DFT predictions for cc-IIIb are compared in Fig. 8a to data from Pippinger et al. (2015). Due to the large number of atoms in the unit cell (50), Raman intensities of cc-III could not be computed. The 75 Raman-active normal mode frequencies are too many to make a useful comparison with the experimental Raman spectra of cc-III and with the spectra of cc-IIIb at lower and higher pressure. The Raman bands of the theoretical spectra of cc-VI are in the wavenumber ranges as observed in our experiments (Fig. 8c). However, the experimental spectra are very broad for these highest pressures. This makes a detailed comparison of the spectra in the low-frequency range below 600 cm^{-1} difficult. The shift of the high frequency band at about 1100 cm^{-1} with pressure is well reproduced.

For comparison with the experimental IR spectra (shown in Figs. 2c, d, 4), Fig. 9 shows the isotropic averages of the imaginary part of the dielectric permittivity tensors from the DFPT calculations for cc-I, cc-IIIb, cc-III and cc-VI. The broad absorption bands in the IR spectra around 1500 and 300-400 cm^{-1} combine a number of vibrational modes. Generally, these groups of modes shift to higher wavenumber with increasing pressure and toward the high-pressure polymorphs. In agreement with experiment, the ν_1 band at around 1100 cm^{-1} that is absent in cc-I shows a distinct splitting for cc-III and less for cc-IIIb at 0 GPa, whereas for cc-IIIb at 10 GPa, a band splitting is barely visible. Due to the different number of atoms in the unit cell, the ν_1 band is composed of five IR-active modes for cc-III, two IR-active modes for cc-IIIb, and a single IR-active mode for cc-VI. A similar mode distribution is observed for the ν_2 band at around 850 cm^{-1} and for the ν_4 band at around 750 cm^{-1}. An

additional band with small intensity appears at somewhat lower wavenumbers (670-700 cm^{-1}) for the cc-III-related phases and for cc-VI. A distinctive feature of cc-VI is the low-frequency mode at about 200 cm^{-1}.

Discussion

Spectra of $CaCO_3$ taken in the cc-III stability field

As shown by Pippinger et al. (2015), the Raman spectra of the cc-IIIb and cc-III polymorphs are very similar and the transition is only indicated in the spectra by a discontinuity in the band shift of the doublet bands and by a splitting of the band around 160 cm^{-1} into two bands (see their Fig. 3).

The splitting of the bands of the doublet around 100 cm^{-1} is much lower below 3.3 GPa then above this pressure, which also holds true for the spectra shown in Figs. 2 and 3. Figure 10 shows the band position *versus* pressure determined from the Raman spectra of four different pressure series. The discontinuity of the band shift and thus the transition from cc-IIIb to cc-III is located between 3 and 4 GPa as determined by Pippinger et al. (2015). It can be seen in the different shifts of the doublet bands around 100 cm^{-1} with pressure (Fig. 10) and in the splitting of the band around 160 cm^{-1} (Fig. 3b, c). It seems that this is the only significant difference between the Raman spectra of cc-IIIb and cc-III. We have a second strong indication for the transition of cc-IIIb to cc-III in the range of 3 to 4 GPa as we observe in the FIR spectra much clearer pattern difference between the spectra at 2.3 GPa (cc-IIIb) and 4.0 GPa (cc-III) than in the Raman spectra (Fig. 2d). The DFT calculations of the dielectric permittivity spectra (Fig. 9) indicate that a distinctive feature of the cc-III phase as compared to cc-IIIb is the splitting of the v_1, v_2 and v_4 bands in the wavenumber range between 600 and 1200 cm^{-1}. This is mainly due to the increased number of atoms in the unit cell. For instance, the v_1 band at about 1100 cm^{-1} is composed of two IR-active modes in cc-IIIb, whereas it consists of five modes in cc-III. However, the quality of the experimental data does not allow resolving such fine details.

We further observed a strong discontinuity in the low-frequency modes of the Raman spectra between 5 and 6 GPa. Such a change was not observed in the infrared spectra: The SR-MIR spectra of the

experiment DAC-HT-18A did show the characteristic cc-III pattern (Williams et al. 1992; Catalli and Williams 2005), but Raman spectra of experiment DAC-HT 18B, which were taken on the same sample, showed the Raman spectral pattern as described above with a missing doublet band and a new band around 120 cm^{-1}.

Using the results from the DFT calculations, we may interpret this second phase transition as a reentrance of the cc-IIIb structure. This unusual behavior is related to a change in compression mechanism of the cc-IIIb phase (see Fig. 7b). At low pressures up to about 3-4 GPa, cc-IIIb has a much higher compressibility than all other studied polymorphs including cc-III. The larger volume stabilizes cc-IIIb with respect to cc-III at low (or slightly negative) pressures. Above 4 GPa, the compression curves of cc-III and cc-IIIb are nearly parallel with cc-IIIb having a slightly higher density (Fig. 7b). The resulting enthalpy curves (Fig. 7a) indicate a limited stability field of cc-III between 0 and 5 GPa. The respective enthalpy differences are very low, but calculations with a generalized gradient approximation functional confirmed this behavior.

To rationalize the structural change in the cc-IIIb structure between low and high pressures, two representative structures are shown in Fig. 11. The major structural difference is a different alignment of the CO_3 groups (indicated by arrows in Fig. 11). Otherwise, both structures look very similar. Due to the low symmetry, there is no change in space group. As all structural and thermodynamic parameters change continuously along the whole pressure range, there is no indication of a phase transition of cc-IIIb.

Transition region between cc-IIIb and cc-VI

In all experiments (Raman, mid-infrared and far-infrared spectroscopy), we observe a transitional region where cc-IIIb and cc-VI coexist and where the cc-VI bands evolve while those of cc-IIIb diminish with increasing pressure. This is very pronounced in the Raman and MIR spectra and less in the FIR- spectra. It seems that there is a kind of transitional region between about 12 and 17 GPa where cc-IIIb slowly transforms to cc-VI (Figs. 3a-c; 4a, a-1, a-2). Catalli and Williams (2005) observed a well-resolved change of the v_4 mode from 2 distinct peaks at 13.5 GPa to four peaks at

higher pressures. Cattali and Williams (2005) interpret these features as co-appearance of cc-III and cc-VI over a broad pressure range due to sluggish and kinetically delayed reaction (see also Santillán 2003). Two of the four bands of the v_4 mode belong to cc-III (690 and 755 cm^{-1} at 10 GPa), and the other two are the new bands for cc-VI (705 and 745 cm^{-1} at 20 GPa). We observe this splitting of the MIR bands for the v_4 mode, but also for v_1 and v_2 (Figs. 4, 6). The transition region can also be seen in the Raman spectra: In the spectra taken at pressures >9.5 GPa, the intense band between 120 and 130 cm^{-1} shifts with increasing pressure to lower wavenumber and starts to decrease in intensity from 12 GPa until it disappears at about 15.3 GPa. In parallel, the characteristic bands for cc-VI at about 150 and 190 cm^{-1} (13.7 GPa) start to increase in intensity from about 14 GPa to about 20 GPa. As mentioned before, the evolution of the far-infrared spectra with pressure is much clearer (Fig. 4b). However, in the spectra above 10 GPa and with increasing pressure, the appearance and growing of a band around 200 and 100 cm^{-1} could be explained as sluggish reaction of cc-IIIb to cc-VI starting between 10 and 11 GPa, and be completed in the spectrum at 19.8 GPa.

The structural phase transition of cc-IIIb to cc-VI

We mostly used the drastic changes of the Raman mode for identifying the phase transition. However experimental reasons, some of the experiments had to be stopped shortly before cc-VI had been formed, we noted those experiments as the transitional region in which the Raman mode of cc-IIIc at 120 cm^{-1} nearly disappeared, but the cc-VI modes not as strong as in the cc-VI field (e.g., spectrum at 13.6 in Fig. According to Catalli and Williams (2005), only the evolution of new v_4 bands in the MIR spectra diagnostic for the transformation of cc-IIIb to cc-VI. However, the transition to cc-VI can be seen in the spectra much clearer than in the MIR spectra (Fig. 4). Adams and Williams (1980) were the first published far-infrared spectra of calcite in a diamond anvil cell up to 0.4 GPa. To our knowledge, no infrared spectra for any carbonate at pressures exceeding 0.5 GPa are reported up to now in the literature no Raman and no far-infrared spectra of cc-VI.

In the in situ experiments at pressures and temperatures, we were able to trace the transition of cc-IIIb to c (Figs. 6, 7) or showed that cc-IIIb (Fig. 5a) or cc-VI (Fig. 5b) remains stable with increasing temperat Some heating experiments started also with the cc-VI structure, and temperature was increased up to 6 (DAC-HT-19).

The results of all experiments are summarized in Table 2 and plotted in a pressure-temperature diagram showing the stability fields of cc-IIIb and cc-VI in Fig. 12. Merlini et al. (2012) speculated that temperature may stabilize the structures of cc-III to lower pressure, and surprisingly, we found the same for the cc-IIIb to cc-VI transition. We have chosen 15 GPa as the transformation pressure of cc-IIIb to cc-VI at ambient temperature as in all pressure series here the main cc-VI pattern were observed in accordance to literature data. The reaction has a negative slope of about -7.0×10^{-3} GPa K^{-1}. As the reaction is kinetically hindered and we observe a transition region, we assume an uncertainty of the slope of about ± 20 %.

Finally, we address the question of whether or not cc-VI may become thermodynamically stable with respect to aragonite at high pressures and temperatures. While cc-VI has a higher density than aragonite, its DFT-derived enthalpy at $T = 0$ K is higher over the whole pressure range studied here (Fig. 7). The only possibility to stabilize cc-VI over aragonite would be a substantial difference in entropy. Assuming that the entropy for a pure phase is dominated by the vibrational part and both structures are built of CO_3^{2-} units and Ca^{2+} cations, a large entropy difference is not expected. Hence, we do not expect cc-VI to become stabilized with respect to aragonite even at high temperatures and mantle pressures. However, further experiments and a more dedicated computational study are needed to provide a more conclusive picture.

Acknowledgments

We thank Reiner Schulz and Andreas Ebert for technical support. We thank HZB for the allocation of synchrotron radiation beamtime. This study was partly supported by a Grant from Deutsche Forschungsgemeinschaft within the Research Unit FOR2125 under Grant KO1260/16. Part of the simulations was performed at the supercomputer JUROPA at Jülich Supercomputing Centre (JSC) within the framework of NIC Grant HPO15. We thank two

anonymous reviewers for their very useful comments and suggestions, which helped to improve the manuscript.

References

Adams DM, Willimas AD (1980) Vibrational spectroscopy at very high pressures. Part 26. An infrared study of the metastable phases of $CaCO_3$. J Chem Soc Dalton 8:1482-1486

Baroni S, de Gironcoli S, Dal Corso A, Giannozzi P (2001) Phonons and related crystal properties from density-functional perturbation theory. Rev Mod Phys 73:515-562

Boulard E, Gloter A, Corgne A, Antonangeli D, Auzende AL, Perrillat JP, Guyot F, Fiquet G (2011) New host for carbon in the deep Earth. PNAS 108:5184-5187

Boulard E, Pan D, Galli G, Liu Z, Mao WL (2015) Tetrahedrally coordinated carbonates in Earth's lower mantle. Nat commun 6:6311

Bridgman PW (1939) The high pressure behavior of miscellaneous minerals. Am J of Sci 237:7-18

Caracas R, Bobocioiu E (2011) The WURM project – a freely available web-based repository of computed physical data for minerals. Am Miner 96:437-443

Carteret C, De la Pierre M, Dossot M, Pascale F, Erba A, Dovesi R (2013) The vibrational spectrum of $CaCO_3$ aragonite: a combined experimental and quantum-mechanical investigation. J Chem Phys 138:014201

Catalli K, Williams Q (2005) A high-pressure phase transition of calcite-III. Am Mineral 90(10):1679-1682

Catalli K, Santillán J, Williams Q (2005) A high pressure infrared spectroscopic study of $PbCO_3$-cerussite: constraints on the structure of the post-aragonite phase. Phys Chem Miner 32(5-6):412-417

Cerantola V, McCammon C, Kupenko I, Kantor I, Marini C, Wilke M, Ismailova L, Solopova N, Chumakov A, Pascarelli S, Dubrovinsky L (2015) High-pressure spectroscopic study of Siderite ($FeCO_3$) with focus on spin crossover. Am Mineral 100:2670-2681

Chaney J, Santillán JD, Knittle E, Williams Q (2014) A high-pressure infrared and Raman spectroscopic study of $BaCO_3$: the aragonite, trigonal and Pmmn structures. Phys Chem Miner 42(1):83-93

Datchi F, Dewaele A, Loubeyre P, Letoullec R, Le Godec Y, Canny B (2007) Optical pressure sensors for high-pressure-high-temperature studies in a diamond anvil cell. High Press Res 27:447-463

Farfan G, Wang S, Ma H, Caracas R, Mao WL (2012) Bonding and structural changes in siderite at high pressure. Am Mineral 97(8-9):1421-1426

Gillet P, Biellmann C, Reynard B, McMillan P (1993) Raman spectroscopic studies of

carbonates part I: high-pressure and high-temperature behaviour of calcite, magnesite, dolomite and aragonite. Phys Chem Miner 20:1-18

Gonze X, Lee C (1997) Dynamical matrices, Born effective charges, dielectric permittivity tensors, and interatomic force constants from density-functional perturbation theory. Phys Rev B 55:10355-10368

Gonze X, Amadon B, Anglade PM, Beuken JM, Bottin F, Boulanger P, Bruneval F, Caliste D, Caracas R, Cote M, Deutsch T, Genovese L, Ghosez P, Giantomassi M, Goedecker S, Hamann DR, Hermet P, Jollet F, Jomard G, Leroux S, Mancini M, Mazevet S, Oliveira MJT, Onida G, Pouillon Y, Rangel T, Rignanese GM, Sangalli D, Shaltaf R, Torrent M, Verstraete MJ, Zerah G, Zwanziger JW (2009) ABINIT: First-principles approach of materials and nanosystem properties. Comput Phys Comm 180:2582-2615

Isshiki M, Irifune T, Hirose K, Ono S, Ohishi Y, Watanuki T, Nishibori E, Takata M, Sakata M (2004) Stability of magnesite and its high-pressure form in the lowermost mantle. Nature 427(6969):60-63

Jahn S, Kowalski PM (2014) Theoretical approaches to structure and spectroscopy of Earth materials. Rev Mineral Geochem 78:691-743

Jamieson JC (1957) Introductory studies of high-pressure polymorphism to 24,000 bars by x-ray diffraction by some comments on calcite II. J Geol 65:334-343

Jing Q, Wu Q, Liu Y, Zhang Y, Liu S, Liu L, J-a Xu, Bi Y (2013) Effect of pressure and temperature on the wavelength shift of the fluorescence line of $SrB_4O_7:Sm^{2+}$ scale. High Press Res 33(4):725-733

Koch-Müller M, Speziale S, Deon F, Mrosko M, Schade U (2011) Stress-induced proton disorder in hydrous ringwoodite. Phys Chem Miner 38(1):65-73

Koch-Müller M, Mrosko M, Gottschalk M, Schade U (2012) Pressure-induced phase transitions in ilvaite studied by in situ micro-FTIR spectroscopy. Eur J Mineral 24(5):831-838

Kraft S, Knittle E, Williams Q (1991) Carbonate stability in the Earth's mantle: a vibrational spectroscopic study of aragonite and dolomite at high pressures and temperatures. J Geophys Res 96(B11):17997-18009

Kulshreshtha C, Cho SH, Jung YS, Sohn K (2006) Deep red color emission in an Sm^{2+}-doped SrB_4O_7 phosphor. Proc ASID 6:294-296

Lin CC, Liu LG (1997) High pressure phase transformations in aragonite-type carbonates. Phys Chem Miner 24:149-157

Liu LG, Mernagh TP (1990) Phase transitions and Raman spectra of calcite at high pressures and room temperature. Am Mineral 75:801-806

Mao HK, Xu J, Bell PM (1986) Calibration of the ruby pressure gauge to 800 kbar under quasi-hydrostatic conditions. J Geophys Res 91:4673-4676

Merlini M, Hanfland M, Crichton WA (2012) $CaCO_3$-III and $CaCO_3$-VI, high-pressure polymorphs of calcite: possible host structures for carbon in the Earth's mantle. Earth Planet Sci Lett 333-334:265-271

Merlini M, Crichton WA, Chantel J, Guignard J, Poli S (2014) Evidence of interspersed co-existing $CaCO_3$ - III and $CaCO_3$ - IIIb structures in polycrystalline $CaCO_3$ at high pressure. Mineral Mag 78(2):225-233

Merrill L, Bassett WA (1975) The high-pressure structure of $CaCO_3$ (II), a high pressure metastable phase of calcium carbonate, Acta Cryst B31:343-349

Minch R, Dubrovinsky L, Kurnosov A, Ehm L, Knorr K, Depmeier W (2010a) Raman spectroscopic study of $PbCO_3$ at high pressures and temperatures. Phys Chem Miner 37(1):45-56

Minch R, Seoung DH, Ehm L, Winkler B, Knorr K, Peters L, Borkowski LA, Parise JB, Lee Y, Dubrovinsky L, Depmeier W (2010b) High-pressure behavior of otavite ($CdCO_3$). J Alloy Compd 508(2):251-257

Mirwald P (1976) A differential thermal analysis study of the high-temperature polymorphism of calcite at high pressure. Contrib Miner Petrol 59:33-40

Mrosko M, Koch-Müller M, Schade U (2011) In-situ mid/far micro-FTIR spectroscopy to trace pressure-induced phase transitions in strontium feldspar and wadsleyite. Am Mineral 96(11-12):1748-1759

Oganov AR, Glass CW, Ono S (2006) High-pressure phases of $CaCO_3$: crystal structure prediction and experiment. Earth Planet Sci Lett 241(1-2):95-103

Oganov AR, Ono S, Ma Y, Glass CW, Garcia A (2008) Novel high-pressure structures of $MgCO_3$, $CaCO_3$ and CO_2 and their role in Earth's lower mantle. Earth Planet Sci Lett 273(1-2):38-47

Perdew JP, Wang Y (1992) Accurate and simple analytic representation of the electron-gas correlation energy. Phys Rev B 45:13244-13249

Perdew JP, Zunger A (1981) Self-interaction correction to density-functional approximations for many-electron systems. Phys Rev B 23:5048-5079

Pippinger T, Miletich R, Merlini M, Lotti P, Schouwink P, Yagi T, Crichton WA, Hanfland M (2015) Puzzling calcite-III dimorphism: crystallography, high-pressure behavior, and pathway of single-crystal transitions. Phys Chem Miner 42(1):29-43

Raju SV, Zaug JM, Chen B, Yan J, Knight JW, Jeanloz R, Clark SM (2011) Determination of the variation of the fluorescence line positions of ruby, strontium tetraborate, alexandrite, and samarium-doped yttrium aluminum garnet with pressure and temperature. J Appl Phys 110(2):023521-023528

Santillán J (2003) Dolomite-II: A high-pressure polymorph of $CaMg(CO_3)_2$. Geophys Res Lett 30(2): 1054. doi:10.1029/2002gl016018

Santillán J, Williams Q (2004) A high-pressure infrared and X-ray study of $FeCO_3$ and $MnCO_3$; comparison with $CaMg(CO_3)_2$-dolomite. Phys Earth Planet Inter 143-144:291-304

Santillán J, Catalli K, Williams Q (2005) An infrared study of carbon-oxygen bonding in magnesite to 60 GPa. Am Mineral 90:1669-1673

Spivak A, Solopova M. Cerantola V, Bykova E, Zakharchenko E, Dubrovinsky L, Litvin Y (2014) Phys Chem Miner 41:633-638

Suito K, Namba J, Horikawa T, Taniguchi Y, Sakurai N, Kobayashi M, Onodera A, Shimomura O, Kikegawa T (2001) Phase relations of $CaCO_3$ at high pressure and high temperature. Am Mineral 86(9):997-1002

Tyburczy JA, Ahrens TJ (1986) Dynamic compression and volatile release of carbonates. J Geophys Res 91(B5):4730-4744

Valenzano L, Noel Y, Orlando R, Zicovich-Wilson CM, Ferrero M, Dovesi R (2007) Ab initio vibrational spectra and dielectric properties of carbonates: magnesite, calcite and dolomite. Theor Chem Acc 117:991-1000

Veithen M, Gonze X, Ghosez P (2005) Nonlinear optical susceptibilities, Raman efficiencies, and electrooptic tensors from first-principles density functional perturbation theory. Phys Rev B71:125107

Wenk, H.-R., Bulakh A. (2004) Minerals. Their constitution and origin. Cambridge University Press. ISBN 0 521 82238 6

White WB (1974) The carbonate minerals. In: Farmer VC (ed) The infrared spectra of minerals. Mineralogical Society Monograph, London, pp 227-279

Williams Q, Collerson B, Knittle E (1992) Vibrational spectra of magnesite (MgCO3) and calcite III at high-pressures. Am Mineral 77:1158-1165

Wittlinger J et al. (1997) High-pressure study of h.c.p.-argon. Acta Crystallogr A B53:745 - 749

Table 1 Vibrational studies of carbonates as a function of temperature and/or pressure

	$CaCO_3$ cc-I	$CaCO_3$ aragonite	Magnesite	Siderite	Dolomite	Strontianite	Cerrusite	Otavite	Witherite
Raman	Liu and Mernagh (1990) Pippinger et al. (2015)	[a]Kraft et al. (1991) Gillet et al. (1993)[a]	Williams et al. (1992) Gillet et al. (1993) Spivak et al. (2014)	Farfan et al. (2012) Spivak et al. (2014) Cerantola et al. (2015)	Kraft et al. (1991) Gillet et al. (1993)[b]	Lin and Liu (1997)	Minch et al. (2010a)	Minch et al. (2010b)	Chaney et al. (2014)
Max. P at T	10 GPa/RT	30 GPa/RT	60 GPa/RT	58 GPa/RT	28 GPa/RT	42 GPa/RT	17 GPa/723 K	40 GPa/RT	45 GPa/RT
Max. T at P	550 K/2.2 GPa	RT[a]	RT	RT	RT[2]	RT	723 K/17 GPa	RT	RT
Mid-IR	Williams et al. (1992) Catalli and Williams (2005)	Kraft et al. (1991)	Williams et al. (1992) Santillan et al. (2005)	Santillan and Williams (2004)	Santillán (2003)	-	Catalli et al. (2005)	-	Chaney et al. (2014)
Max. P at T	52 GPa/RT	40 GPa/RT	60 GPa/RT	50 GPa/300 K	50 GPa/RT		41 GPa/RT		45 GPa/RT
Max. T at P	RT	RT	RT	RT	RT		RT		RT
Far-IR	This study Adams and Williams (1980)	-	-	-	-	-	-	-	
Max. P at T	26.5 GPa/RT								
Max. T at P	RT								

[a]Kraft et al. 1991 took Raman spectra after laser heating to 2100 K at 30 GPa
[b]Kraft et al. 1991took Raman spectra after externally heating to 550 K at 10 GPa

Table 2 Experimental conditions and results

Run	Method	*P* (GPa)	*T* (K)	Phase	Run	Method	*P* (GPa)	*T* (K)	Phase
DAC-HT-15[a,e]	Raman	15.3	300	cc-VI	DAC-HT-18B	Raman	12.3	726	*Transition*
"	"	15.0	300	cc-VI	"	"	13.3	681	*Transition*
"	"	14.7	300	*Transition*[d]	DAC-HT-12	MIR	19.4	324	cc-VI
M2-FIR-I[b]	SR-FIR	26.5	300	cc-VI	"	"	"	363	"
M2-FIR-II[b]	"	28.6	300	cc-VI	"	"	18.1	389	"
DAC-HT-18A	Sr-MIR	16.9	300	cc-VI	DAC-HT-22[e]	Raman	13.6	516	*Transition*
DAC-HT-13C	Raman	>14.5	300	cc-VI	"	"	13.5	520	"
M3-17[c]	Raman	12.3	300	cc-IIIb	"	"	13.7	543	cc-VI
M2-MIR-I[c]	MIR	20.3	300	cc-VI					
ZHS-MIR-II[c]	MIR	21.9	300	cc-VI	"	"	13.8	450	cc-IIIb
DAC-HT-19[e]	Raman	14.1	427	*Transition*	"	"	14.7	494	cc-VI
"	"	11.9	714	"	"	"	15.0	522	cc-VI
"	"	13.8	533	"	DAC-HT-16	Raman	11.9	388	cc-IIIb
"	"	14.1	400	"	"	"	11.3	342	"
"	"	15.4	658	cc-VI	"	"	11.8	548	"
"	"	14.2	443	"	"	"	11.2	475	"
"	"	14.9	481	"	"	"	9.8	468	"
"	"	12.7	512	cc-IIIb	DAC-HT-21	Raman	9.8	512	cc-IIIb
"	"	12.1	448	"	"	"	9.9	450	"
"	"	14.1	412	"	DAC-HT-6	SR-MIR	10.5	499	cc-IIIb
"	"	14.0	375	"	"	"	9.8	512	"
DAC-HT-18B	"	13.2	512	"	"	"	9.9	450	"

[a] All experiments in the DAC-HT used NaCl as pressure medium and the cell were relaxed by annelaing using the internal heater to 70 to 100 °C at low pressures

[b] Petroleum jelly was used as pressure medium

[c] Argon was used as pressure medium; if necessary, the cell was annealed at 8 GPa to 120 °C for 0.5 h

[d] "*transition*" means that the P-T conditions are close to the transformation of cc-III to cc-VI, indicated by disappearance of the Raman band around 120 cm-1 and before the appearance of the two bands at 150 and 200 cm-1, which are indicative for cc-VI

[e] In these experiments, the phase boundary cc-IIIb-cc-VI was crossed several times and on their base the slope of the transition has been determined

Table 3 Lattice parameters and unit cell volumes of cc polymorphs from DFT calculations

Phase	P (GPa)	a (Å)	b (Å)	c (Å)	α (°)	β (°)	γ(°)	V (Å^3)
cc-I	0	5.001	5.001	16.661	90	90	120	360.94
cc-I	2	4.984	4.984	16.383	90	90	120	352.47
cc-I	5	4.969	4.969	15.969	90	90	120	341.44
cc-III	0	6.282	7.514	12.553	93.652	98.765	106.78	557.04
cc-III	5	6.200	7.301	12.401	93.290	98.535	107.17	527.31
cc-III*	5	6.197	7.276	12.395	93.210	98.610	106.95	525.43
cc-III	10	6.133	7.135	12.271	92.977	98.278	107.44	504.39
cc-III	20	6.013	6.901	12.025	92.633	97.595	107.63	469.42
cc-IIIb	-2	6.221	6.439	6.424	94.458	106.28	105.50	234.77
cc-IIIb	-1	6.187	6.412	6.406	94.255	106.78	105.99	230.60
cc-IIIb	0	6.152	6.390	6.389	94.063	107.31	106.58	226.46
cc-IIIb*	0	6.129	6.380	6.385	93.755	107.70	106.53	224.82
cc-IIIb	1	6.114	6.375	6.375	93.911	107.95	107.62	221.69
cc-IIIb	2	6.085	6.365	6.357	93.871	108.54	108.61	217.25
cc-IIIb	3	6.065	6.353	6.337	93.920	108.94	109.11	214.03
cc-IIIb	4	6.049	6.340	6.319	93.944	109.21	109.39	211.50
cc-IIIb	5	6.034	6.327	6.301	93.989	109.48	109.56	209.22
cc-IIIb*	5	6.022	6.333	6.300	93.896	109.86	109.63	208.28
cc-IIIb	10	5.973	6.266	6.225	94.301	110.50	110.07	199.84
cc-IIIb*	10	5.969	6.276	6.228	94.345	110.90	110.03	199.50
cc-IIIb	20	5.890	6.151	6.111	94.951	112.03	110.40	186.23
cc-VI	5	3.456	5.090	5.943	100.59	96.364	90.053	102.09
cc-VI	10	3.413	5.016	5.815	101.61	95.365	89.743	97.096
cc-VI	20	3.374	4.894	5.636	102.77	94.581	89.487	90.462
cc-VI*	20	3.388	4.881	5.632	102.88	94.479	89.410	90.529

*Results from LDA pseudopotentials using Perdew and Wang (1992) functional (ABINIT option ixc = 7). All other calculations used pseudopotentials with ixc = 2 (LDA according to Perdew and Zunger (1981)). Ixc = 7 is required for calculation of Raman spectra

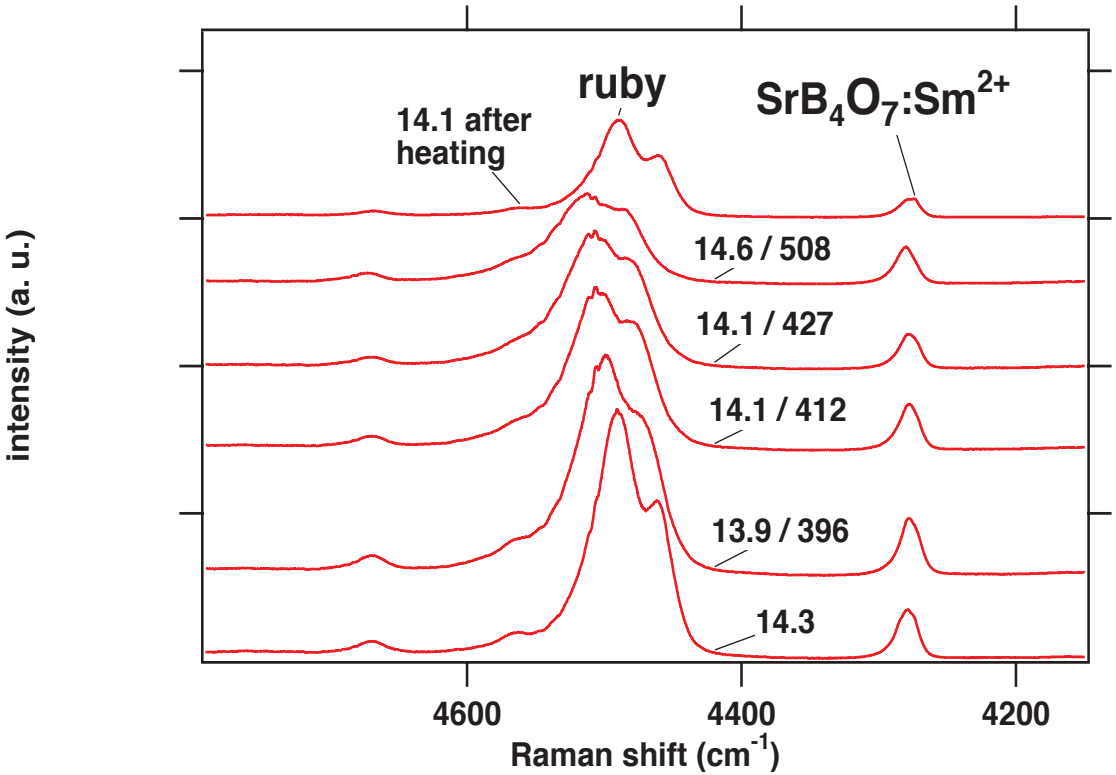

Fig. 1 Representative fluorescence spectra of ruby and $SrB_4O_7:Sm^{2+}$ taken at about 14 GPa and up to 510 K. The energy scale is given as Raman shift from the excitation green laser light (18,791 cm^{-1})

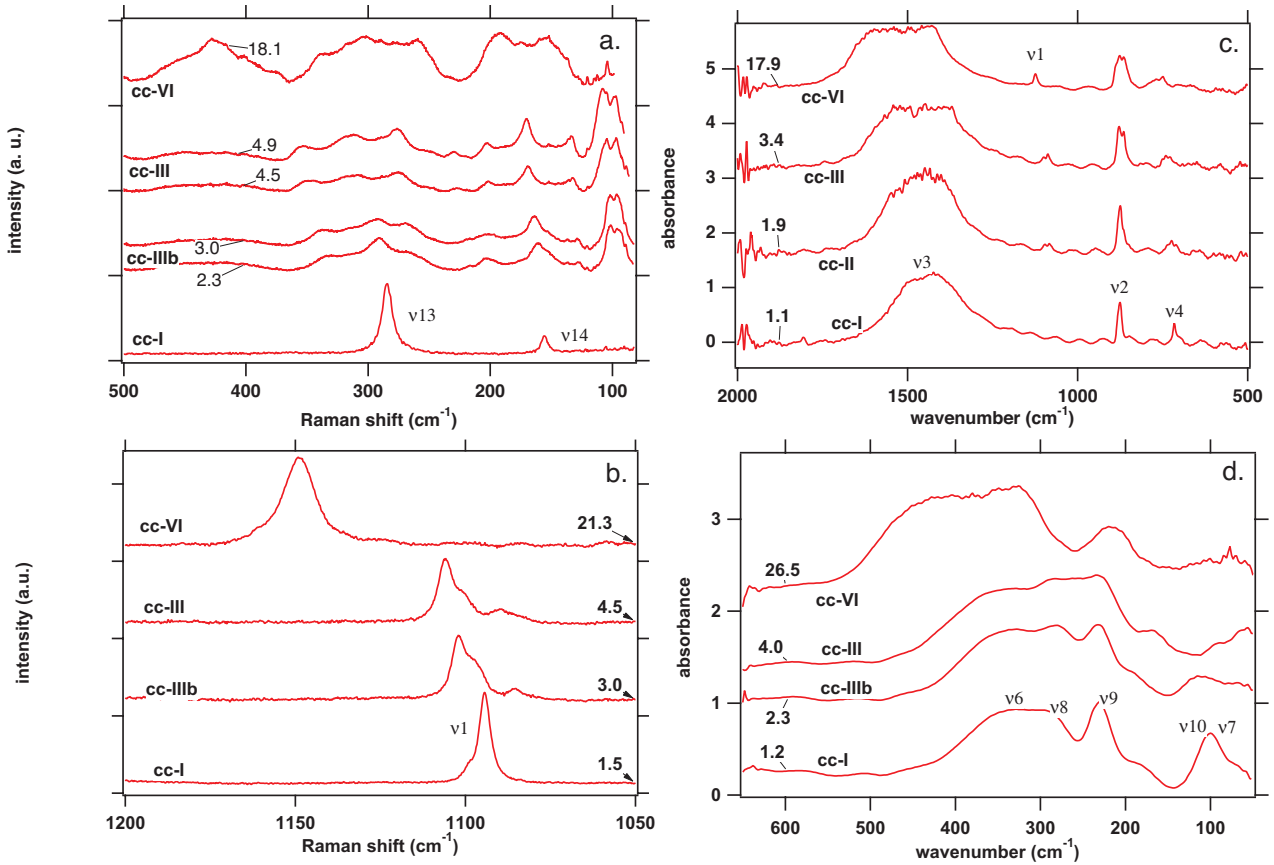

Fig. 2

Fig. 2 Vibrational characteristics of the $CaCO_3$ polymorphs **a** Raman spectra from 75 to 500 cm^{-1}, **b** Raman spectra from 1000 to 1200 cm^{-1} **a**, **b** both experiment DAC-HT-15, **c** mid-infrared spectra (M2-MIR-1), **d** far-infrared spectra (M2-FIR-1). Figures denote pressure in GPa; the spectra are offset for clarity

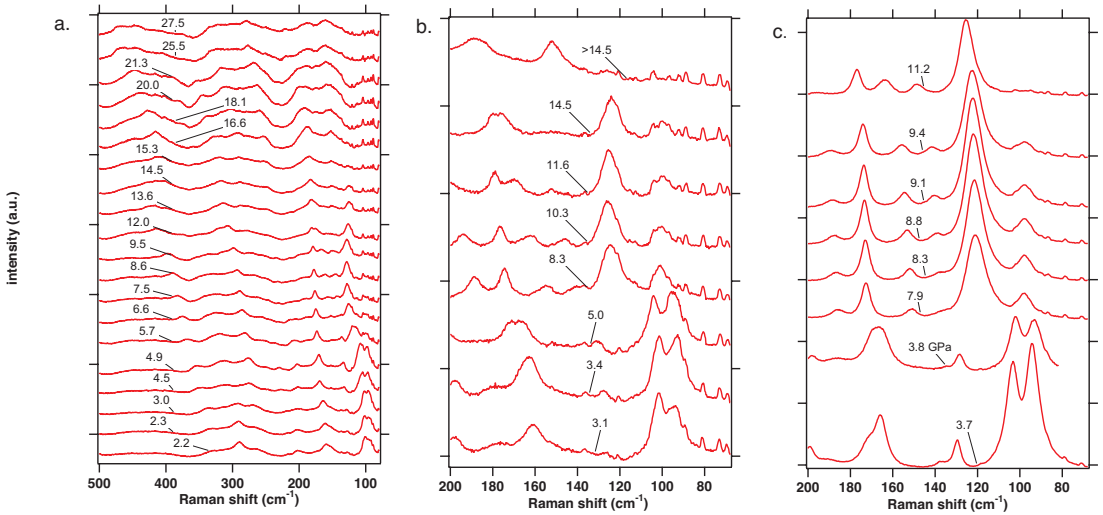
a.
b.
c.
intensity (a.u.)
27.5
25.5
21.3
20.0
18.1
16.6
15.3
14.5
13.6
12.0
9.5
8.6
7.5
6.6
5.7
4.9
4.5
3.0
2.3
2.2
>14.5
14.5
11.6
10.3
8.3
5.0
3.4
3.1
11.2
9.4
9.1
8.8
8.3
7.9
3.8 GPa
3.7
500 400 300 200 100
200 180 160 140 120 100 80
Raman shift (cm-1)

Fig. 3 a-c

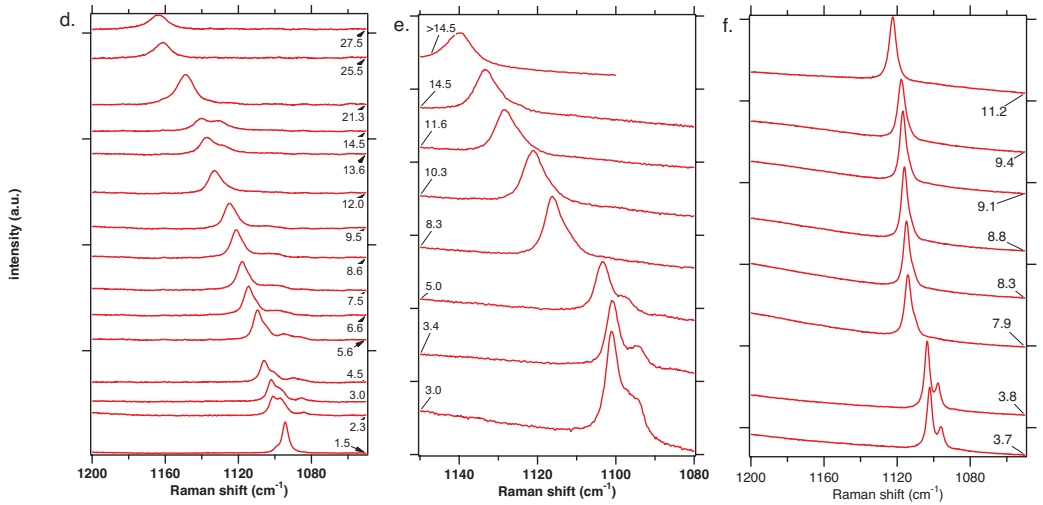

Fig. 3 d-f

Fib. 3

Fig. 3 Pressure-induced evolution of the vibrational changes at ambient temperature. **a**, **d** Raman spectra with a natural calcite containing 1 mol% of magnesite as starting material (DAC-HT-15); **c**, **f** Raman spectra with a natural calcite containing 1 mol% of magnesite as starting material (DAC-HT-16), **b**, **e** Raman s pectra with pure calcite as starting material (DAC-HT-13C); here, the exact pressure for cc-VI transition cannot be specified as we were no longer able to measure the fluorescence spectrum of ruby. The abrupt change in the low-frequency range of the spectra between 3.9 GPa (cc-III) and 7.6 is explained by a re-appearance of cc-IIIb at the expense of phase cc-III, visible only in the Raman spectra. The change is also visible in the high-frequency spectra by the disappearance of the low-energy shoulder of the ν_1 mode. Figures denote pressure in GPa; spectra are offset for clarity

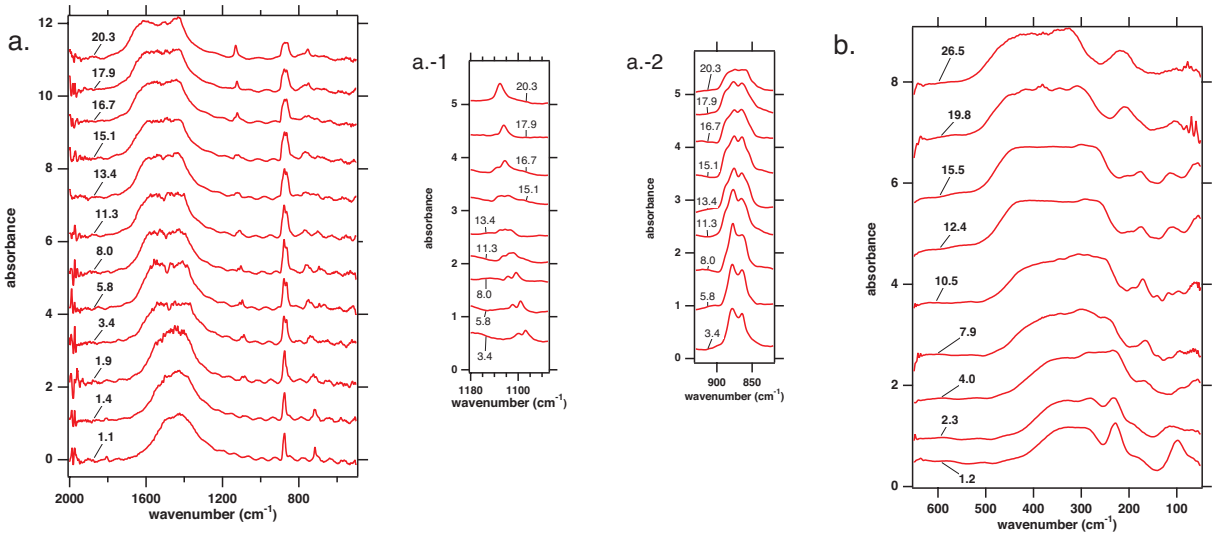

Fig. 4

Fig. 4 Pressure-induced evolution of the vibrational changes at ambient temperature in **a** mid-infrared spectra taken on a thin film of pure $CaCO_3$ (M2-MIR-I) and details for v_1 (*a.-1*) and v_2 (*a.-2*); **b** far-infrared spectra taken on a thin film of pure $CaCO_3$ (M2-FIR-I). Figures denote pressure in GPa and spectra are offset for clarity

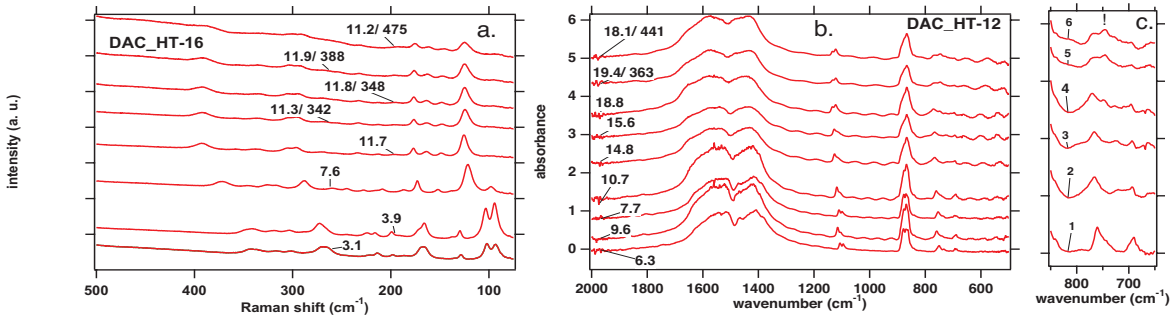

Fig. 5

Fig. 5 a Raman spectra taken on calcite as starting material in the stability field of cc-III (DAC-HT-16). Temperature increase to 475 K at about 12 GPa does not promote the transformation to cc-VI. **b** mid-infrared spectra taken on a thin calcite film showing the transition of cc-III to cc-VI (DAC-HT-12). Different to Fig. 4b the ν_1 mode of cc-VI is here a doublet, and the ν_2 mode tends to become a singlet as proposed by Catalli and Williams (2005), but not observed in our mid-infrared experiments in Fig. 4b. This indicates the complex nature of the phase transitions of $CaCO_3$. **c** Zoom of six spectra of Fig. 4b starting with 1 4.8 GPa (*1*) and ending at 18.1 GPa and 441 K (*6*) showing the evolution of a new band (!) of the ν_4 mode, which is indicative for the transition of cc-III to cc-VI. Figures denote pressure in GPa; spectra are offset for clarity

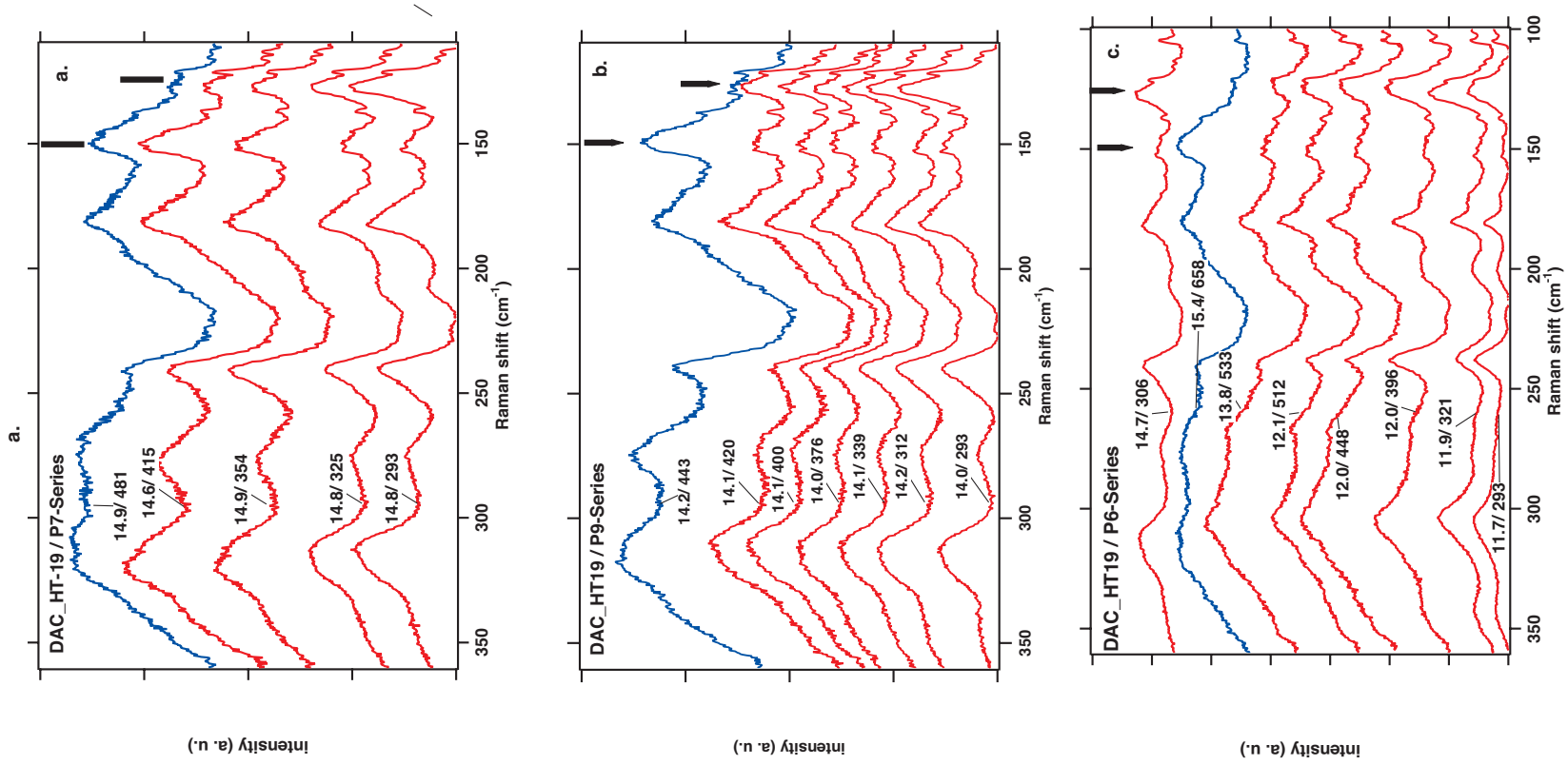

Fig 6-feb15

Fig. 6 Three series of in situ Raman spectra as a function or pressure and temperature (DAC-HT-19); the spectra in *blue* show the first appearance of cc-VI. Cc-VI Raman spectra are characterized by the disappearance of the vibrational mode at around 120 cm^{-1} and the appearance of an intense band at 150 cm^{-1}. Shortly before the structure transforms, we observe a kind of transitional region where the two bands at 130 and 150 cm^{-1} became both very low in intensity. **c** The cc-VI spectrum has been taken at 15.4 GPa and 658 K, and after temperature release, cc-VI transforms immediately to cc-IIIb (spectrum at 14.7 GPa and 306 K)

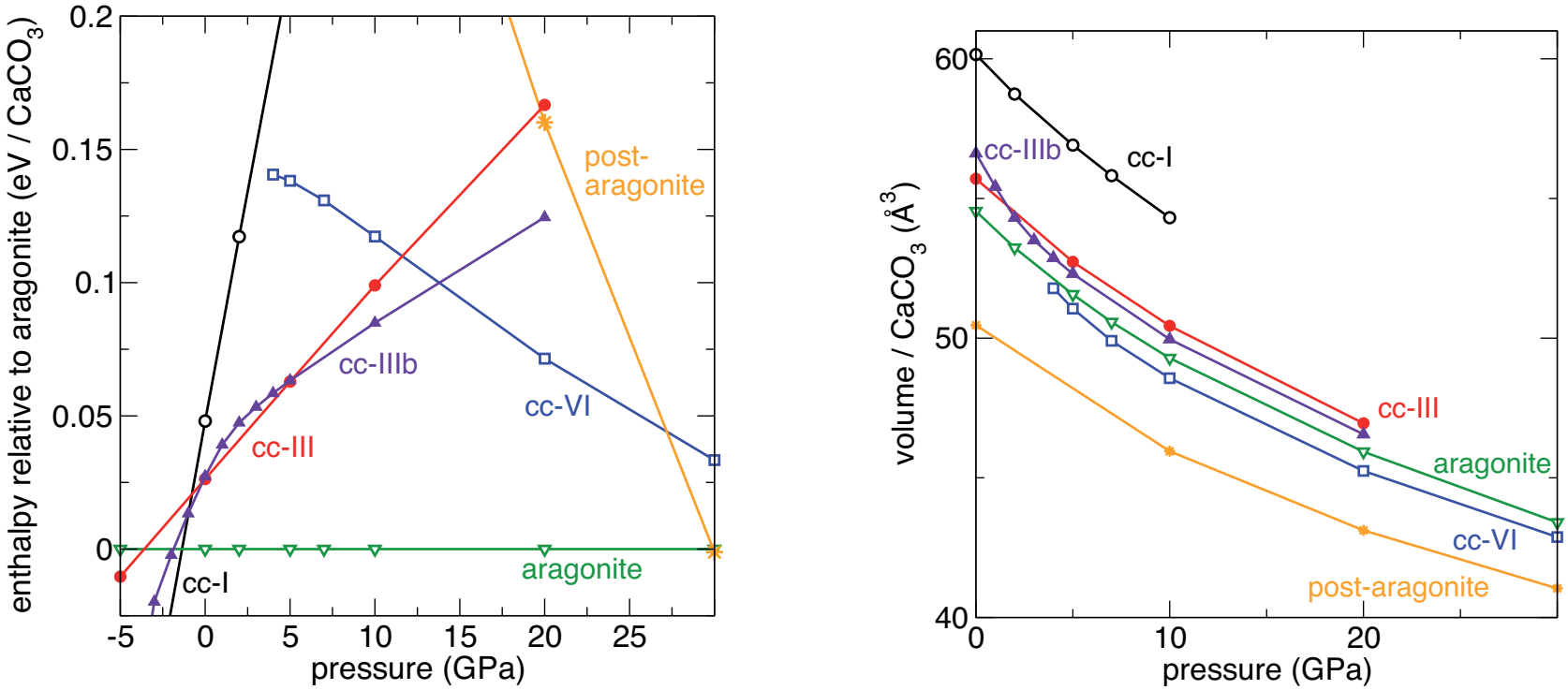

Fig. 7 a Enthalpies and **b** volumes of different $CaCO_3$ phases from the DFT calculations

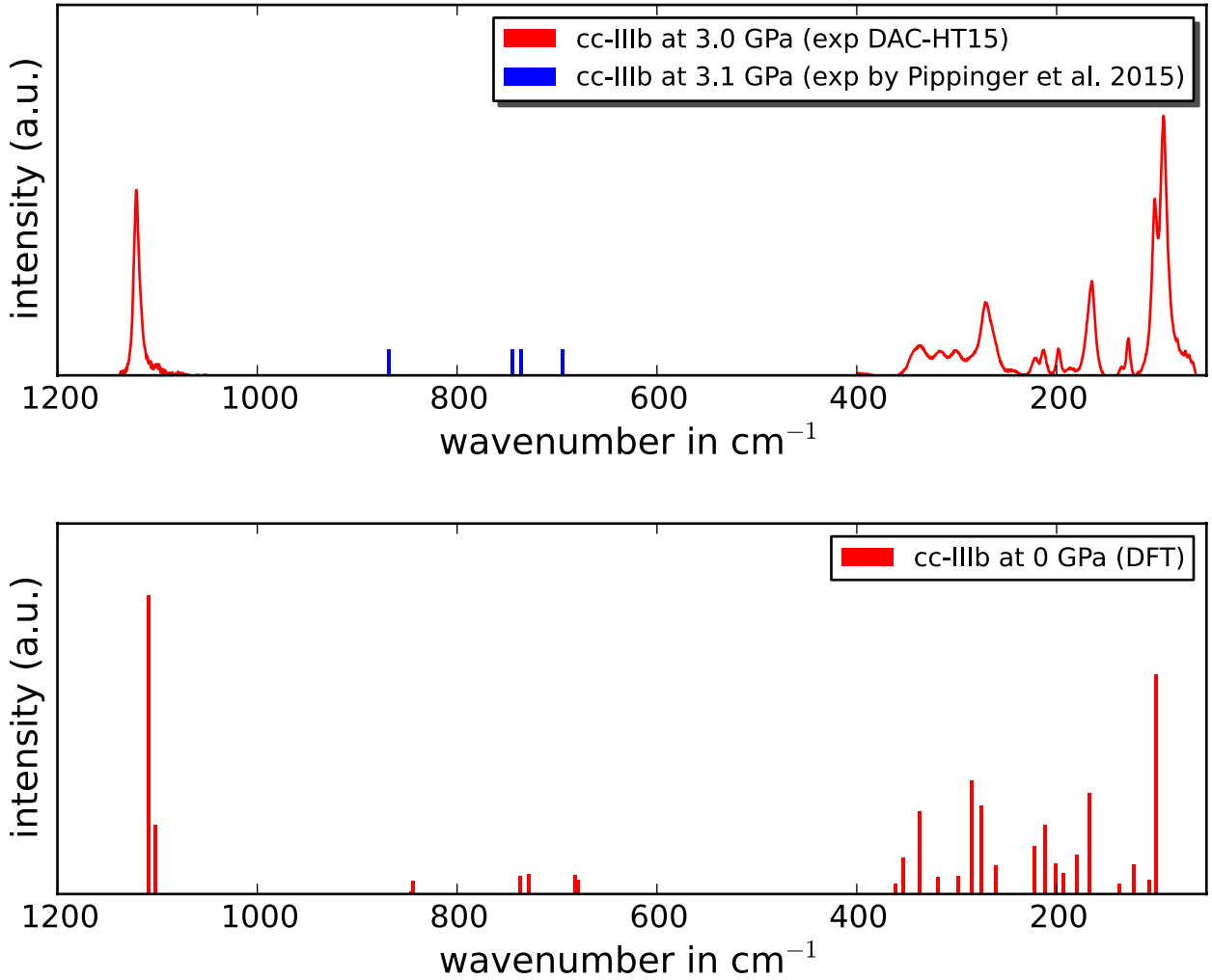
cc-IIIb at 3.0 GPa (exp DAC-HT15)
cc-IIIb at 3.1 GPa (exp by Pippinger et al. 2015)
intensity (a.u.)
1200
1000
800
600
400
200
wavenumber in cm^{-1}
cc-IIIb at 0 GPa (DFT)
intensity (a.u.)
1200
1000
800
600
400
200
wavenumber in cm^{-1}

Fig.8a

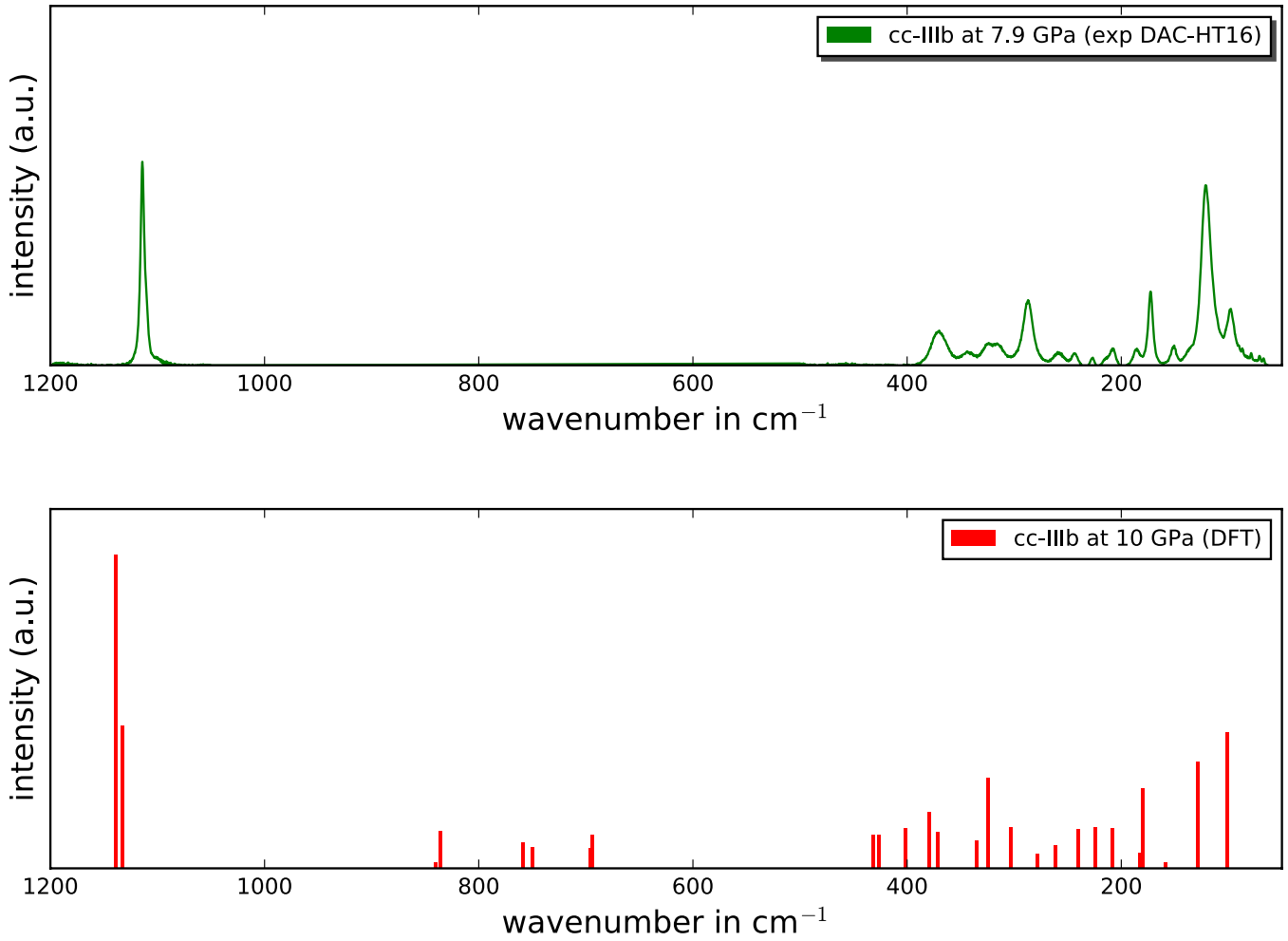
cc-IIIb at 7.9 GPa (exp DAC-HT16)
intensity (a.u.)
1200
1000
800
600
400
200
wavenumber in cm^{-1}
cc-IIIb at 10 GPa (DFT)
intensity (a.u.)
1200
1000
800
600
400
200
wavenumber in cm^{-1}

Fig.8b

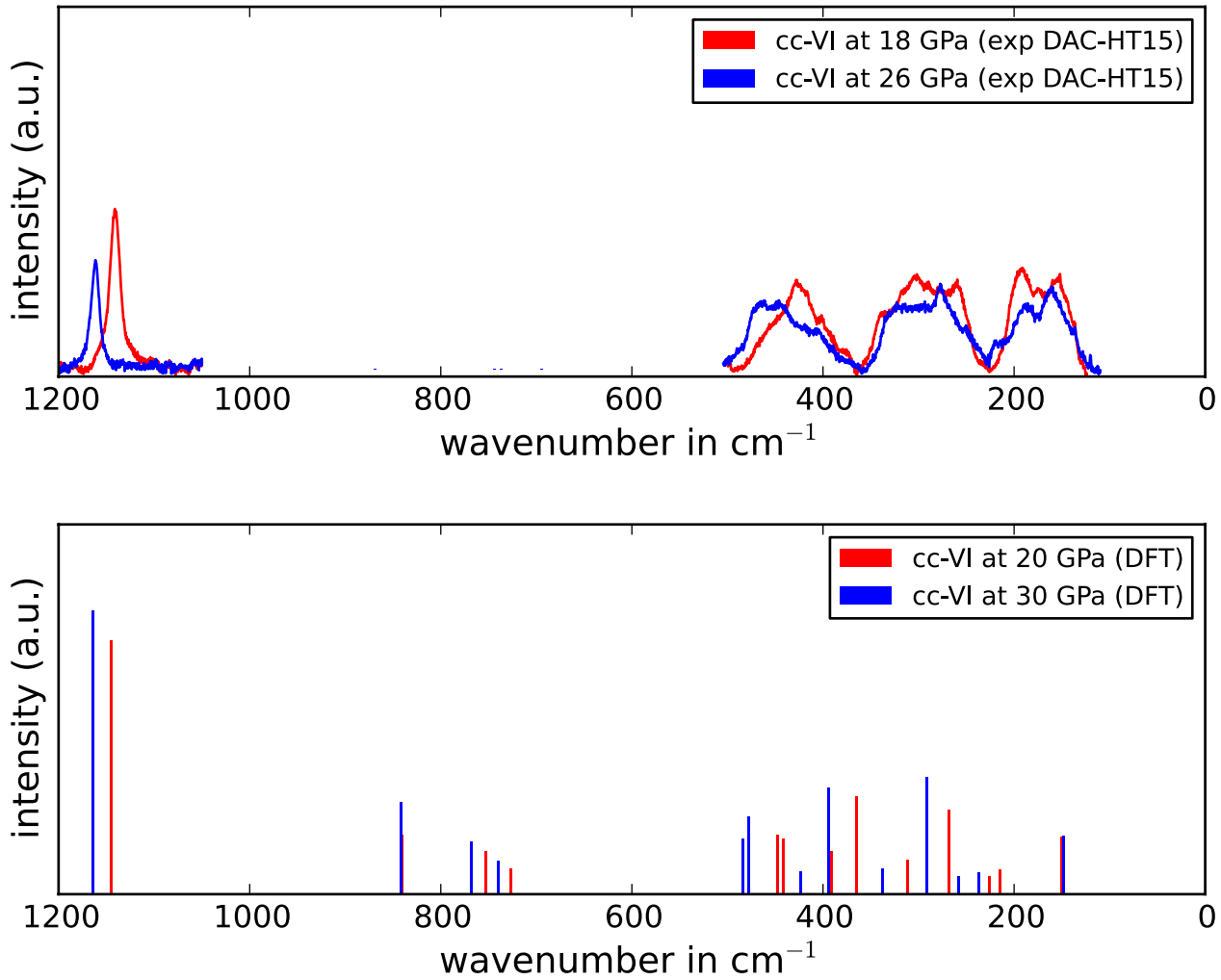

Fig.8c

Fig. 8 Comparison of theoretical and experimental Raman spectra for cc-IIIb (**a**, **b**) and cc-VI (**c**)

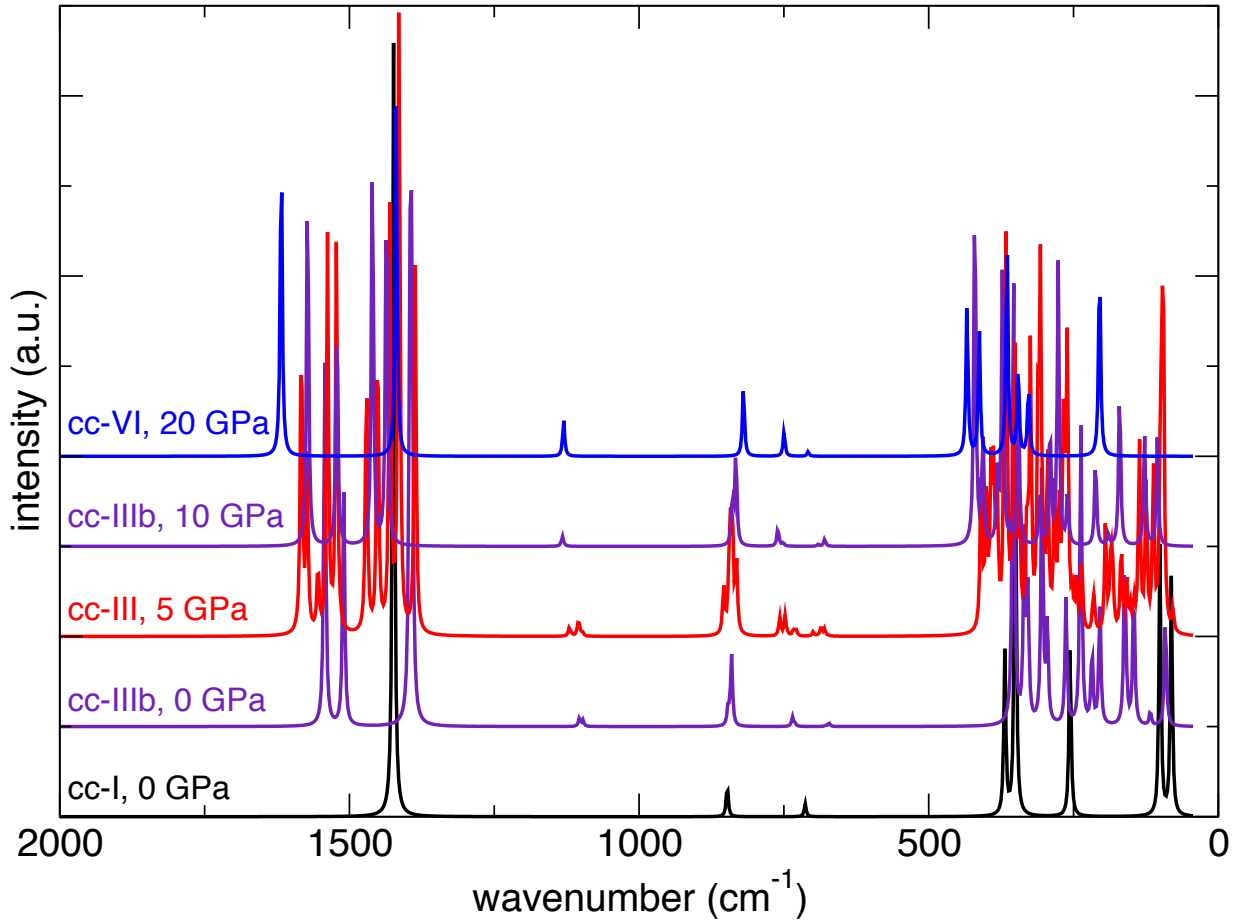

Fig. 9 Vibrational spectra obtained from the imaginary part of the dielectric permittivity for different cc structures from DFPT

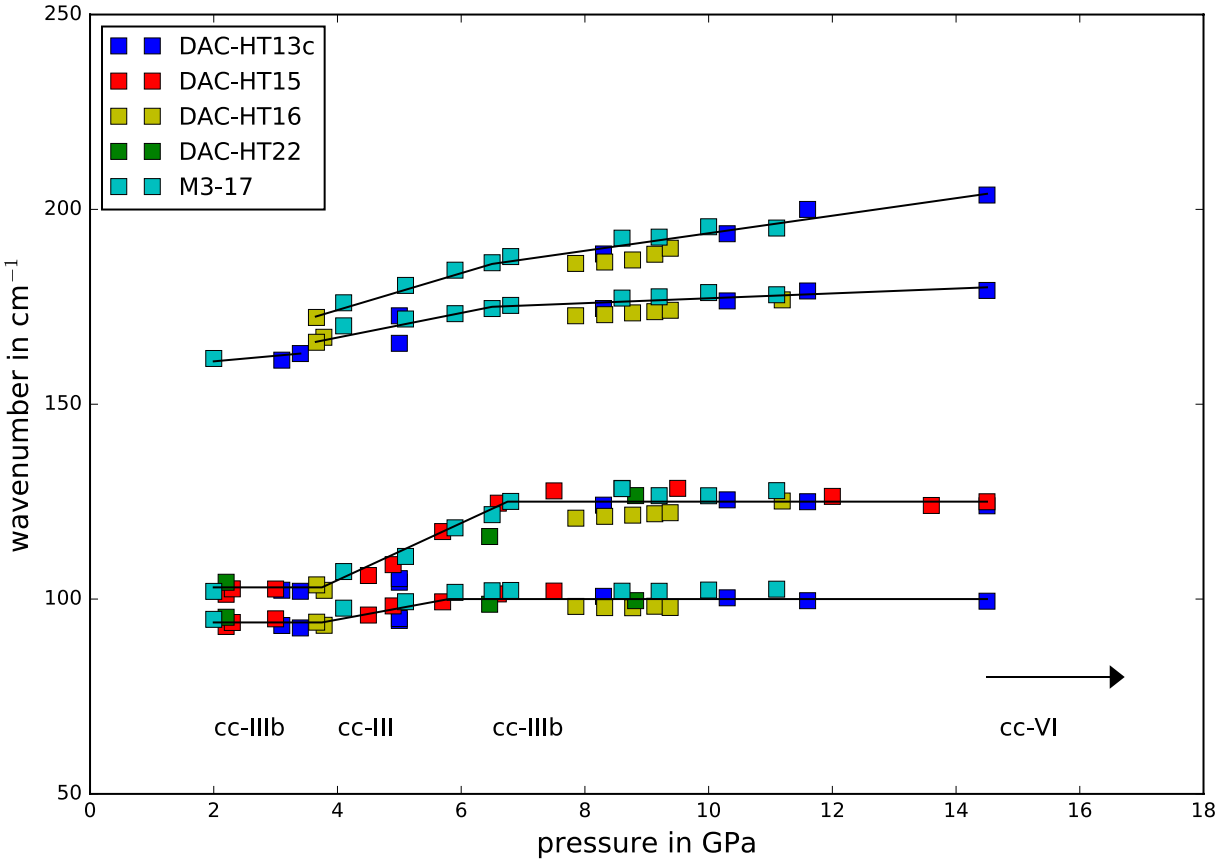

Fig. 10 Plot of the wavenumber of the low-frequency modes of the Raman spectra as a function of pressure at ambient temperature

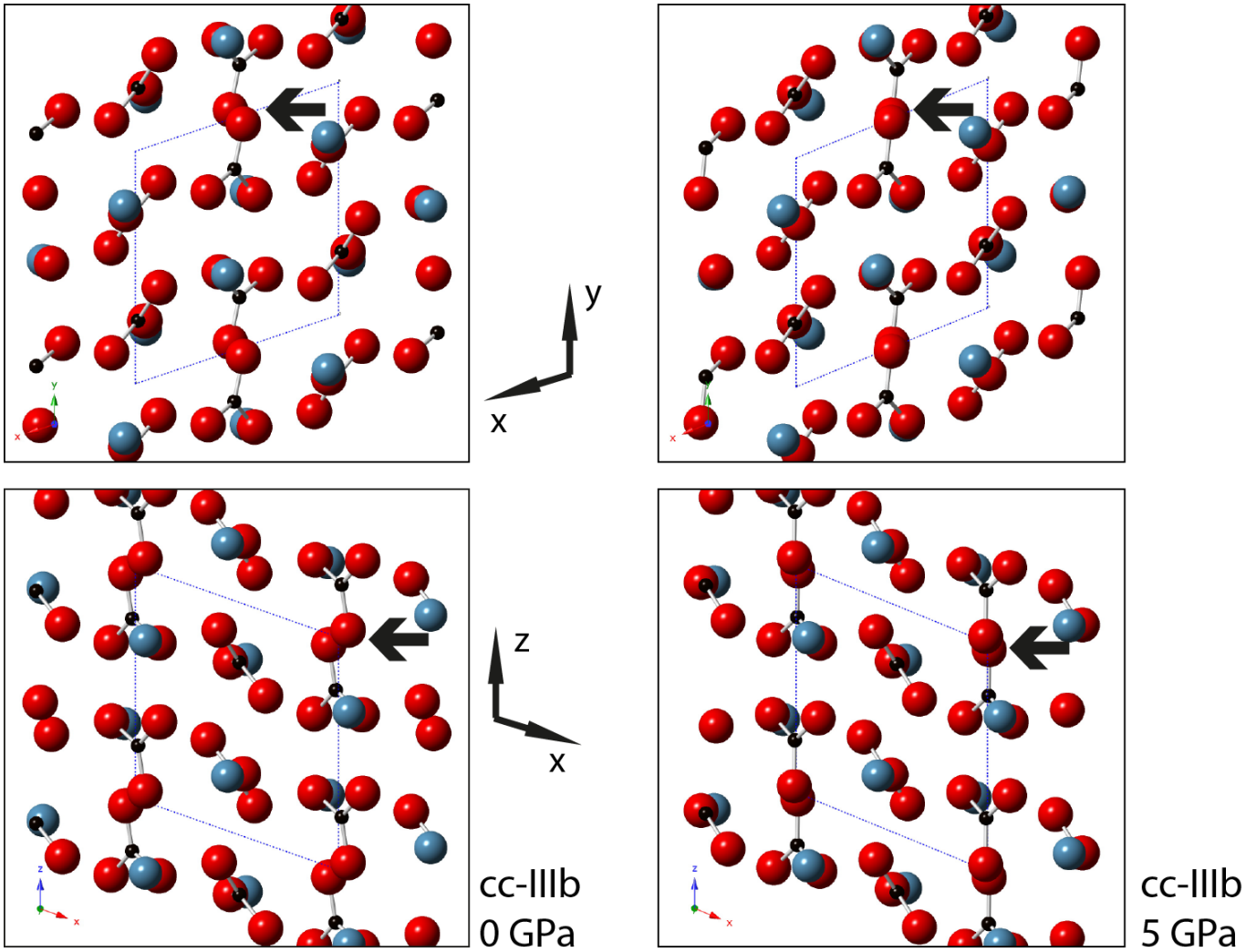

Fig. 11 DFT-derived structures of cc-IIIb at low pressure (*left*) and high pressure (*right*) projected along crystallographic z-axis (*top*) and y-axis (*bottom*). The main structural differences are indicated by *arrows*

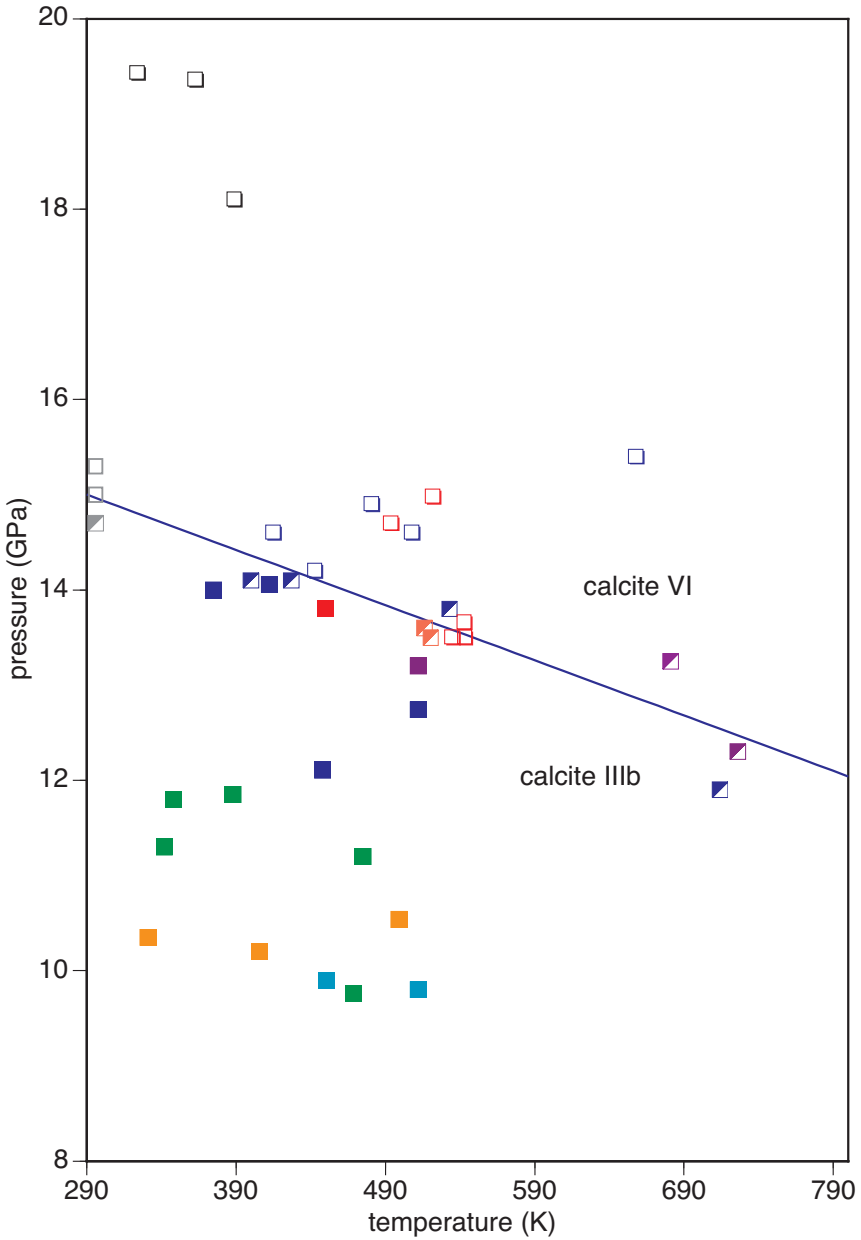
20
18
16
14
12
10
8
pressure (GPa)
290
390
490
590
690
790
temperature (K)
calcite VI
calcite IIIb

Fig.12 P-T diagram showing the cc-IIIb and cc-VI stability field as determined by in situ vibrational spectroscopy. For the different experiments, we used different *colours*: DAC-HT-6 *orange*; DAC-HT-12 *black*; DAC-HT-15 *grey*; DAC-HT-16 *green*; DAC-HT-18B *purple*; DAC-HT-19 blue; DAC-HT-21 *bluish green*; DAC-HT-22 *red*. The *open symbols* of each *colour* represent the stability of cc-VI, *closed symbols* the stability of cc-IIIb, and half-filled symbols the transition region. In the experiments DAC-HT-15, 19, and 22, the phase boundary cc-IIIb-cc-VI was crossed several times, and on their base, the slope of the transition has been determined to -7×10^{-3} GPa K^{-1}. As the reaction is kinetically hindered and we observe a transition region, we assume an uncertainty of the slope of about ± 20%